To cite this version :

Riadh OUZANI, Sofiane KHELLADI, Xesús NOGUEIRA - High thermal Rayleigh number with double-diffusive finger convection: Effect of nonlinear equation of state - International Communications in Heat and Mass Transfer - Vol. 158, p.107861 - 2024

High thermal Rayleigh number with double-diffusive finger convection: Effect of nonlinear equation of state

OUZANI Riadh[1], KHELLADI Sofiane[2], NOGUEIRA Xesus[3]

[1]LESEI Laboratory, Mechanical Engineering Department, University of Batna 2, Fesdis, Algeria.
[2]Arts et Métiers Institute of Technology, CNAM, LIFSE, HESAM University, F-75013 Paris, France
[3]Group of Numerical Methods in Engineering-GMNI, Center for Technological Innovation in Construction and Civil Engineering-CITEEC, Universidade da Coruña, Civil Engineering School, Campus de Elviña, 15071, A Coruña, Spain.

Abstract

In this study, we numerically investigate the effects of the nonlinearity in the equation of state on the structure of fingers and the transport mechanisms of salt and heat in double-diffusive finger convection, utilizing the finite volume approach with high-accuracy schemes to solve the two-dimensional Navier–Stokes equations. Our system is characterized by a low buoyancy ratio and a high thermal Rayleigh number, with density variation modeled as quadratic in temperature and linear in salinity. Three cases of nonlinear parameters were examined: the linear case ($\varepsilon = 0$), weak nonlinear case ($\varepsilon = 1$), and highly nonlinear case ($\varepsilon = 3$).

It is shown that increasing the nonlinear parameter enhances the buoyancy force acting on descending fingers more than on ascending ones, resulting in narrower and faster-growing descending fingers. Conversely, ascending fingers are appreciably damped, growing more slowly but with greater width. This asymmetry in finger development gives rise to distinct convective patterns between the upper and lower layers, significantly influencing the formation of mixed layers. The mixing process was also examined by analyzing the probability density function of salinity PDF(S*). Our findings reveal that as the nonlinear parameter increases, the amount of salt transported by descending fingers from the upper to the lower layer decreases. This reduction in salt transport indicates a corresponding decline in mixing efficiency with higher values of the nonlinear parameter.

Key words: Salt-fingers; double-diffusive convection; Density inversion; Buoyancy ratio.

1. Introduction

Double-diffusion convection into fingering configurations frequently occurs in most aquatic environments and plays a significant role in the vertical transport of salt and heat, as well as in the upwelling of nutrients in lakes, seas, and oceans [1-3]. In such environments, the interplay between the different diffusion rates of heat and salt leads to the formation of intricate convective patterns. This double-diffusive process can also take place in many engineering systems composed of two or multiple components with different molecular diffusivities. Examples include solar ponds, which are large-scale energy storage systems that use saltwater to collect and store solar energy. In these ponds, the upper layer is less salty and cooler, while the bottom layer is hotter and saltier. Double-diffusion convection helps to stabilize the temperature gradient and prevent the mixing of layers, thus maintaining the pond's ability to store heat [4]. In CO_2 sequestration, CO_2 is injected into saline aquifers for long-term storage. Understanding double-diffusive convection is crucial for predicting the mixing and movement of CO_2 within the aquifer. The interaction between the injected CO_2 (which is less dense and less viscous) and the saline water (which is denser and more viscous) can lead to fingering patterns that enhance mixing and storage efficiency [5]. Double-diffusive convection in magma chambers can also lead to the formation of a finger interface between layers of different composition and temperature. This occurs when a layer of hot, slightly less dense magma overlies a cooler, denser, but compositionally lighter magma. In such cases, compositional differences are transported downwards faster than heat, influencing processes like fractional crystallization, assimilation, and magma mixing. The formation and behavior of these finger structures are influenced by chamber geometry, magma density, and viscosity variations, ultimately affecting the composition of erupted or solidified products [6]. In stellar radiative regions, double-diffusion convection plays a role in the transport of energy and matter. The differential diffusion of heat and helium can create fingering structures that affect the mixing and stability of stellar interiors, influencing stellar evolution and the formation of various stellar phenomena [7]. In geothermal systems, the interaction between hot, saline geothermal fluids and cooler, less saline fluids can create convective patterns that enhance the efficiency of heat extraction and the sustainability of geothermal reservoirs [8]. Many industrial chemical processes rely on the controlled mixing of substances with different diffusivities. Double-diffusive convection can be harnessed to improve mixing efficiency, enhance reaction rates, and optimize the production of chemicals [9].

In the past few years, considerable research efforts have been devoted to the study of double-diffusive convection. This phenomenon has attracted and continues to attract the interest of many scientists and industrialists. Recently, the effect of double diffusion has been studied in various configurations, such as peristaltic transport [10], [11], [12], [13], nanofluids [14], [15], [16], non-Newtonian fluids [17], [18], [19], [20], and magneto-rheological fluids [21], [22], [23], [24]. Additional recent research on double diffusion in mixed convection can be found in references [25], [26], [27], [28], [29].

Under appropriate circumstances, when the temperature stratification of fluid in the lower layer with a faster diffuser (T) is stabilizing and the salinity stratification of fluid in the upper layer with a slower diffuser (S) is destabilizing, in such a flow situation instability can be developed in the form of a set of alternative narrow or wide vertical cellular structures of upward, cold fresh fluid and downward, hot salty fluid [30], [31]. These structures named double-diffusive salt fingers.

In the past years, extensive research, theoretical [32–34], numerical [35–37] and experimental [38–40], have been focused on the buoyancy flux ratio R_f variation associated with the fingering convection systems. In terms of modeling, the majority of the previous studies assumed the buoyancy flux ratio R_f law is related only on the density stability ratio [49-52] Nevertheless, the principal deficiency in all these formulations of these models is ignoring the Rayleigh number effect.

Over the past two decades, there has been a significant interest in studying the effect of Rayleigh numbers on double-diffusive salt fingers, which has posed new challenges for the scientific community. Taylor and Veronis [39], have been the first to implicitly point out the importance of the salinity Rayleigh number as a key parameter on the flux ratio R_f and on the evolution salt finger system by controlling the magnitude of the salt anomaly. Later, by using numerical simulations, Shen and Veronis [41] have been discussed the effect of the thermal and salinity Rayleigh numbers. They have shown that these dimensionless parameters are necessary to express the buoyancy flux ratio R_f produced by fingers; however, they did not provide any details about the nature of the relationship that relate them. In an effort to consolidate perspectives from previous studies, Sreenivas et al. [42] aggregated findings regarding the buoyancy flux ratio's variation as a function of the density stability ratio, as reported in works by various investigators (Turner [43], Özgökmen et al. [44], Schmitt [45], McDougall and Taylor [46], Kelly [47], Kunze [48], Boyd and Perkins [49], Taylor and Bucens [50], Shen [51, 52]). Despite their attempt, they found it challenging to interpret these results due to their considerable scatter. Consequently, they concluded that the density stability ratio alone is insufficient as a parameter to fully explain the flux transport produced by fingers. Through his investigation, it was also discovered that the reason for this huge difference is that these experiments were conducted at different Rayleigh numbers. In order to address this issue, they have been performed a series of two-dimensional numerical studies to investigate the effect of the thermal Rayleigh number Ra_T for a wide range of R_p on the finger width, velocity, and fluxes in double-diffusive fingering convection. They concluded that vertical velocity in the fingers and the flux ratio are a function of both Ra_T and R_p. Additionally, they also indicate that the number of fingers increases with an increase in the thermal Rayleigh number, and at large thermal Rayleigh numbers, the fingers structures become hair-like thin.

Moreover, a crucial dynamic aspect of double-diffusive fingering convection observed at high thermal Rayleigh numbers was the formation of mixed layers. These mixed layers play a significant role in the dynamics and evolution of the salt finger structures, thereby influencing the mixing behavior. It was observed that when mixed layers form, finger structures are sandwiched between them, giving rise to the so-called "fingering zone". Singh and Srinivasan [53] have been given further details about the formation of mixed layers. They show that mixed layers are initially characterized by intense horizontal convection, creating impenetrable layers that limit the growth of fingers. Subsequently, the intensity of convection decreases over time, allowing fingers to penetrate into the mixed layers. Similar findings have been also detailed by Ouzani et al. [54]. It should be noted that at low thermal Rayleigh numbers, fingers evolve without the formation of mixed layers.

In the aforementioned works, the fluid system's temperature is far from the temperature of maximum density; hence the numerical simulations of the double-diffusive salt fingers are commonly studied in a simplified model that satisfies Oberbeck–Boussinesq approximation based on the linear equation of state. This simplification assumes that the behavior of the salt finger system, including growth, dynamics, and mixing processes, is identical with respect to the mid-height of the computational domain, leading to vertically symmetric evolution of the finger system.

However, in extremely cold aquatic environments, where temperatures near the maximum density point can approach freezing, the thermal expansion coefficient may change sign, and the Oberbeck-Boussinesq approximation based on the linear temperature-density relationship becomes invalid see [55], [56]. Thus, in such circumstances, the non-Oberbeck–Boussinesq approach is necessary to correctly analyze salt fingering convection. Few numerical simulation studies have been conducted to explore the effect of the nonlinear equation of state on salt fingers dynamics. These studies use a nonlinear model that is quadratic in temperature and linear in salinity. Laboratory experiments reported by McDougall [57] and Schmitt [58] demonstrate that salt finger convection is modified and becomes more intricate, with convective motion developing asymmetrically. Özgökmen and Esenkov [59] showed that complications arise in the double-diffusion salt finger system when the temperature dependence becomes nonlinear. They explored the initial evolution of fingers as a function of the nonlinearity parameter, defined as $\varepsilon = 2\beta_{T_2}\Delta T / \beta_{T_1}$ where β_{T_1} and β_{T_2} are the expansion coefficients corresponding to the linear and nonlinear terms. It is worth noting that their study neglects the interaction of the convective finger structures with boundaries.

More recently, Ouzani and Khelladi [60] conducted numerical simulations to better understand the influence of density inversion on finger dynamics and mixing characteristics of the double diffusive systems. They discovered that the top-down symmetry feature of the finger system breaks as the nonlinearity parameter increases, resulting in asymmetric ascending and descending of finger structures. By utilizing the probability density function of salinity, the authors showed that the nonlinear parameter enhances mixing properties in the lower layer compared to the upper layer.

It should also be mentioned that the works [59], [60] have been limited to the moderate thermal Rayleigh number and density stability ratio, indeed, the flow pattern was not fully described. Further, to the authors' knowledge, there is still a lack of research on the double-diffusive fingering convection under cold ambient conditions. This raises questions about how fingers can interact in cold ambient conditions. In this context, to complement our previous research [60] on double-diffusive finger convection in cold saline systems, we aim to investigate the effect of density inversion induced by the nonlinear equation of state on finger structures' dynamics, their interactions, and the mixed layers at high thermal Rayleigh numbers and low density stability ratio. Special attention is given to analyzing the mixing process using the probability density function.

The remainder of this paper is organized as follows. In section 2, we will present the physical description of the problem, governing equations and we briefly give the high-resolution numerical scheme WENO5 which has the ability to capture the narrow finger structures that generated at high thermal Rayleigh number. Next, we will present our simulation results and discuss the impact of the nonlinear equation of state on the salt-finger convection evolution and mixing characteristics in section 3. Finally, we will offer the principal conclusions in section 4.

2. Mathematical model and numerical procedures

2.1. Mathematical model

We consider a rectangular enclosure wherein width and height are given as B and H respectively, as depicted in figure 1 a. The enclosure contains two distinct uniform fluid layers separated by an interface of finite thickness. The upper layer holds a hot, salty fluid, while the lower layer contains a cold, fresh fluid. This configuration leads to the development of alternating ascending and descending finger structures within the computational domain. The interface between the two layers exhibits a gradient where the temperature and salinity transition smoothly, as shown in figure 1b. In the upper layer, the fluid has a thermal diffusivity denoted by k_T. In the lower layer, the fluid exhibits a higher salinity diffusivity, k_s, where k_T (where $k_T > k_s$).

The key to the salt-fingering instability is the fact that, on molecular scales, heat diffuses much more rapidly than salt. When a parcel of warm, saline water moves downward, it cools off via molecular diffusion of heat while exchanging very little salt. This cooling increases the parcel's density, providing a downward buoyancy force that reinforces its initial downward motion. Similarly, an upward-moving parcel gains heat from the surroundings, becomes lighter, and continues to rise. The net effect is a vertical exchange of water containing salt, creating a downward salt flux. While the heat flux is also directed down-gradient, it is much smaller since most of the heat diffuses out sideways to adjacent parcels, see figure 1b. This combination of heat and salt fluxes yields a density flux that is also downward.

In the present study, we assume that the thermophysical properties of both the salty and fresh fluid remain constant, except for the density variation, which is assumed to be nonlinear with temperature. We adopt the non-Oberbeck-Boussinesq relationship used by Özgökmen and Esenkov [59] to express the density of the fluid, which is given by:

$$\rho(T,S) = \rho_0\left[1-\beta_{T_1}(T-T_0)+\beta_S(S-S_0)-\beta_{T_2}(T-T_0)^2\right] \qquad (1)$$

Where T_0, S_0 and ρ_0 are the reference temperature, salinity and density, respectively. The variation of the density induced by the temperature variation is defined by linear and nonlinear terms associated with thermal expansion coefficients β_{T_1} and β_{T_2}, while β_S is the linear saline contraction coefficient.

To facilitate the analysis of the effect of this nonlinear density relationship on the salt finger system, we introduce the nonlinear parameter which expressed as: $\varepsilon = 2\beta_{T_2}\Delta T / \beta_{T_1}$.

All boundaries of the computational domain are taken to be adiabatic with no salt fluxes across them. Non-slip boundary conditions were applied on the top and bottom of the domain, while slip boundary conditions were applied to the left and right boundaries of the domain. For the initial conditions ($t^* = 0$), the fluid is considered stationary consisting of two layers, whose warm and salty water ($T^* = S^* = 1$) and the lower one contains cold and fresh water ($T^* = S^* = 0$) (see figure1 a).

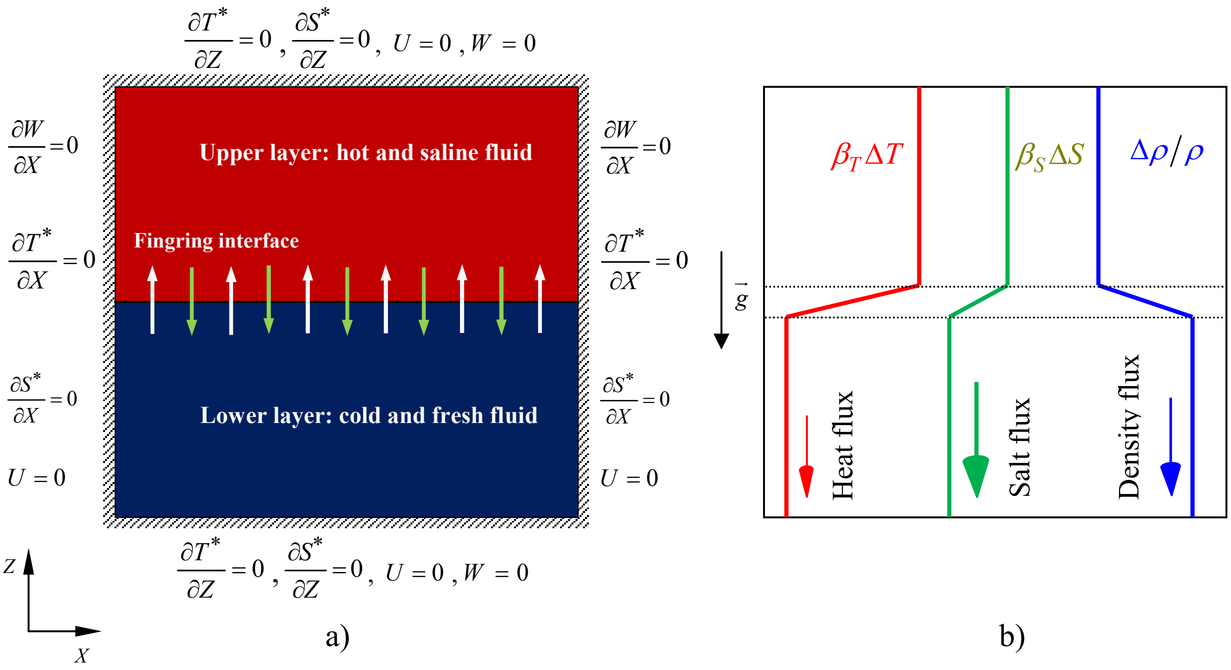

a)

b)

Figure1. A detailed illustration of the double-diffusive system: a) Schematic representation of the physical configuration, coordinate system, and initial and boundary conditions. The sketch outlines the setup with two distinct fluid layers, highlighting the interface, and indicates the imposed conditions at the boundaries and the coordinates used for the analysis. b) Background stratification observed during a "rundown" salt-fingering experiment. The net fluxes, depicted schematically, represent the net fluxes, which are proportional to the differences between the initial (dashed lines) and final (solid lines) profiles of the solute concentrations.

The two-dimensional governing equations (mass, momentum, energy and species) for the double-diffusive system are given as follows [42], [60], [61]:

$$\frac{\partial u}{\partial x}+\frac{\partial w}{\partial z}=0 \tag{2}$$

$$\frac{\partial u}{\partial t}+u\frac{\partial u}{\partial x}+w\frac{\partial u}{\partial z}=-\frac{1}{\rho_0}\frac{\partial p}{\partial x}+\nu(\frac{\partial^2 u}{\partial x^2}+\frac{\partial^2 u}{\partial z^2}) \tag{3}$$

$$\frac{\partial w}{\partial t}+u\frac{\partial w}{\partial x}+w\frac{\partial w}{\partial z}=-\frac{1}{\rho_0}\frac{\partial p}{\partial z}+\nu\left(\frac{\partial^2 w}{\partial x^2}+\frac{\partial^2 w}{\partial z^2}\right)-\left(1-\beta_{T_1}(T-T_0)+\beta_S(S-S_0)-\beta_{T_2}(T-T_0)^2\right)g \tag{4}$$

$$\frac{\partial T}{\partial t}+u\frac{\partial T}{\partial x}+w\frac{\partial T}{\partial z}=k_T(\frac{\partial^2 T}{\partial x^2}+\frac{\partial^2 T}{\partial z^2}) \tag{5}$$

$$\frac{\partial S}{\partial t}+u\frac{\partial S}{\partial x}+w\frac{\partial S}{\partial z}=k_S(\frac{\partial^2 S}{\partial x^2}+\frac{\partial^2 S}{\partial z^2}) \tag{6}$$

Where (u,w) are the velocity components, T, p and S are temperature, pressure and concentration of fluid, respectively. ν , k_T and k_S are the kinematic viscosity, thermal and concentration diffusivity, respectively.

	thermal diffusivity	**salinity diffusivity**	**thermal expansion coefficient**	**salinity expansion coefficient**	**kinematic viscosity**	**domain height**	**aspect ratio**
Unity	k_T $[m^2 s^{-1}]$	k_S $[m^2 s^{-1}]$	β_{T_1} $[{}^0C^{-1}]$	β_S $[s^{-1}]$	ν $[m^2 s^{-1}]$	H $[m]$	$Ar = B/H$
Values	1.4×10^{-7}	1.4×10^{-9}	2×10^{-4}	8×10^{-4}	1.0×10^{-6}	0.15	2

Table 1- Thermophysical properties of the double diffusive system.

The corresponding dimensionless governing equations system is given as follows [60]:

$$\frac{\partial U}{\partial X}+\frac{\partial W}{\partial Z}=0 \tag{7}$$

$$\frac{\partial U}{\partial t^*}+U\frac{\partial U}{\partial X}+W\frac{\partial U}{\partial Z}=-\frac{\partial P}{\partial X}+\Pr(\frac{\partial^2 U}{\partial X^2}+\frac{\partial^2 U}{\partial Z^2}) \tag{8}$$

$$\frac{\partial W}{\partial t^*}+U\frac{\partial W}{\partial X}+W\frac{\partial W}{\partial Z}=-\frac{\partial P}{\partial Z}+\Pr(\frac{\partial^2 W}{\partial X^2}+\frac{\partial^2 W}{\partial Z^2})+\Pr(Ra_T\ T^*(1+\frac{\varepsilon}{2}T^*)-Ra_S S^*) \tag{9}$$

$$\frac{\partial T^*}{\partial t^*}+U\frac{\partial T^*}{\partial x}+W\frac{\partial T^*}{\partial Z}=\left(\frac{\partial^2 T^*}{\partial X^2}+\frac{\partial^2 T^*}{\partial Z^2}\right) \tag{10}$$

$$\frac{\partial S^*}{\partial t^*}+U\frac{\partial S^*}{\partial X}+W\frac{\partial S^*}{\partial Z}=\frac{\Pr}{Sc}\left(\frac{\partial^2 S^*}{\partial X^2}+\frac{\partial^2 S^*}{\partial Z^2}\right) \tag{11}$$

The scaling parameters used to develop the above dimensionless governing equations (7-11) are defined as follows [42] :

$$X=\frac{x}{H},\ Z=\frac{z}{H},\ t^*=\frac{tk_T}{H^2},\ U=\frac{uH}{k_T},\ W=\frac{wH}{k_T},\ \ P=\frac{pH^2}{k_T^2\rho_0},T^*=\frac{T-T_B}{\Delta T},\ S^*=\frac{S-S_B}{\Delta S}$$

where X and Z are the dimensionless Cartesian coordinates in the horizontal and vertical directions, respectively, t^* is the dimensionless time, U and W are the dimensionless velocity components, P is the dimensionless pressure, T^* is the dimensionless temperature and S^* is the dimensionless salinity. T_T and T_B are the temperature of top and bottom layers, $\Delta T=T_T-T_B$, and $\Delta S=S_T-S_B$ are the temperature and the salinity differences between the top and bottom layers.

The classical dimensionless parameters are: Prandtl number $\Pr=\frac{\nu}{k_T}$, Schmidt's number $Sc=\frac{\nu}{k_S}$, thermal Rayleigh number $Ra_T=\frac{g\beta_{T_1}\Delta TH^3}{\nu k_T}$, and salinity Rayleigh number $Ra_S=\frac{g\beta_S\Delta SH^3}{\nu k_S}$.

For the initial conditions ($t^*=0$), the fluid is considered stationary and a step profile across a horizontal interface at mid-depth ($Z=0.5$) is imposed for both temperature and salinity:

$$(U,W)=(0,0)$$
$$T^*(X,t^*=0)=\begin{cases}\Delta T & \text{for } Z\geq 0\\ 0 & \text{for } Z<0\end{cases} \tag{12}$$
$$S^*(X,t^*=0)=\begin{cases}\Delta S & \text{for } Z\geq 0\\ 0 & \text{for } Z<0\end{cases}$$

We chose typical values for the Prandtl number ($\Pr=7$) and the Schmidt number ($Sc=700$), which are commonly used in studies of seawater systems (e.g., [62], [63]). For all simulations, we maintain fixed values for the buoyancy ratio $R_\rho=1.5$, thermal Rayleigh number $Ra_T=7\times10^8$ and salinity Rayleigh number $Ra_S=4.667\times10^8$.

2.2. Computational procedures

As shown by Sreenivas et al. [42], at very high Rayleigh numbers, the number of fingers increases and their dimensions become extremely thin, making them very difficult to detect, which is the main challenge in computational prediction of the evolution of the double-diffusion finger system. It should also be noted that the system is characterized by discontinuity at the interface between two layers in the initial state. Therefore, the numerical schemes should be chosen carefully to accurately capture the thinner fingers structures, their spatio-temporal evolution as well as their interaction with boundaries~~.~~

The numerical methodology employed to solve the dimensionless Navier–Stokes equations (8-11) is described as follows:

- **Approximation of the convective and the diffusive terms**

The tow-dimensional diffusion-convection equations (8-11) are rewritten as:

$$\frac{\partial f}{\partial t^*}=L(f) \tag{13}$$

$$L(f) = A\left(\frac{\partial^2 f}{\partial X^2} + \frac{\partial^2 f}{\partial Z^2}\right) - U\frac{\partial f}{\partial X} - W\frac{\partial f}{\partial Z} + D = \phi_{diff^n_{i,j}} + \phi_{conv^n_{i,j}} + D \tag{14}$$

where $L(f)$ is a spatial discretization operator and f indicates the velocity component (U, W), the temperature T^*, the salinity S^* and D is the term source.

The second partial derivatives $\frac{\partial^2 f}{\partial X^2}$, $\frac{\partial^2 f}{\partial Z^2}$ in the diffusive terms ($\phi_{diff^n_{i,j}}$) are discretized using central differencing with fourth-order accuracy, whereas the spatial discretization of the first partial derivatives $\frac{\partial f}{\partial X}$, $\frac{\partial f}{\partial Z}$ in the nonlinear convective terms ($\phi_{conv^n_{i,j}}$) are approximated by using the fifth-order WENO scheme [64], [65] as follow:

We calculate the smoothness indicators $IS_i, i = 0,1,2$.

The IS_i^+ are given by:

$$IS_0^+ = \frac{13}{12}(f^+_{j-2} - 2f^+_{j-1} + f^+_j)^2 + \frac{1}{4}(f^+_{j-2} - 4f^+_{j-1} + 3f^+_j)^2, \tag{15}$$

$$IS_1^+ = \frac{13}{12}(f^+_{j-1} - 2f^+_j + f^+_{j+1})^2 + \frac{1}{4}(f^+_{j-1} - f^+_{j+1})^2, \tag{16}$$

$$IS_2^+ = \frac{13}{12}(f^+_j - 2f^+_{j+1} + f^+_{j+2})^2 + \frac{1}{4}(3f^+_j - 4f^+_{j+1} + f^+_{j+2})^2, \tag{17}$$

And the IS_i^- are given by:

$$IS_0^- = \frac{13}{12}(f^-_{j+1} - 2f^-_{j+2} + f^-_{j+3})^2 + \frac{1}{4}(3f^-_{j+1} - 4f^-_{j+2} + f^-_{j+3})^2, \tag{18}$$

$$IS_1^- = \frac{13}{12}(f^-_j - 2f^-_{j+1} + f^-_{j+2})^2 + \frac{1}{4}(f^-_j - f^-_{j+2})^2, \tag{19}$$

$$IS_2^- = \frac{13}{12}(f^-_{j-1} - 2f^-_j + f^-_{j+1})^2 + \frac{1}{4}(f^-_{j-1} - 4f^-_j + 3f^-_{j+1})^2, \tag{20}$$

We compute the nonlinear stencil weights :

$$\alpha_i^{\pm} = \frac{d_i}{(\varepsilon + IS_i)^2}, i = 0,1,2$$

Here we choose $\sigma = 10^{-6}$ to avoid the denominator to become zero. The linear weights are given by:

$$d_0 = \frac{1}{10},\ d_1 = \frac{6}{10},\ d_2 = \frac{3}{10}$$

and

$$\alpha_0^{\pm} = \frac{1}{10}\left(\frac{1}{\sigma + IS_0^{\pm}}\right)^2, \quad \alpha_1^{\pm} = \frac{6}{10}\left(\frac{1}{\sigma + IS_1^{\pm}}\right)^2, \quad \alpha_2^{\pm} = \frac{3}{10}\left(\frac{1}{\sigma + IS_2^{\pm}}\right)^2 \tag{21}$$

In order to get a convex combination of ENO stencils, the WENO stencil weights are normalized to give:

$$\omega_0^{\pm} = \frac{\alpha_0^{\pm}}{\alpha_0^{\pm} + \alpha_1^{\pm} + \alpha_2^{\pm}}, \quad \omega_1^{\pm} = \frac{\alpha_1^{\pm}}{\alpha_0^{\pm} + \alpha_1^{\pm} + \alpha_2^{\pm}}, \quad \omega_2^{\pm} = \frac{\alpha_2^{\pm}}{\alpha_0^{\pm} + \alpha_1^{\pm} + \alpha_2^{\pm}} \tag{22}$$

where: $\omega_j^{\pm} \in (0,1)$, $j = 0,1,2$, and $\omega_0^{\pm} + \omega_1^{\pm} + \omega_2^{\pm} = 1$

Finally, the numerical fluxes are defined as:

$$\begin{aligned}\hat{f}^{+}_{j+\frac{1}{2}} &= \omega_0^{+}\left(\frac{2}{6} f^{+}_{j-2} - \frac{7}{6} f^{+}_{j-1} + \frac{11}{6} f^{+}_{j}\right) + \omega_1^{+}\left(-\frac{1}{6} f^{+}_{j-1} + \frac{5}{6} f^{+}_{j} + \frac{2}{6} f^{+}_{j+1}\right) \\ &+ \omega_2^{+}\left(\frac{2}{6} f^{+}_{j} + \frac{5}{6} f^{+}_{j+1} - \frac{1}{6} f^{+}_{j+2}\right)\end{aligned} \tag{23}$$

and

$$\begin{aligned}\hat{f}^{-}_{j+\frac{1}{2}} &= \omega_2^{-}\left(-\frac{1}{6} f^{-}_{j-1} + \frac{5}{6} f^{-}_{j} + \frac{2}{6} f^{-}_{j+1}\right) + \omega_1^{-}\left(\frac{2}{6} f^{-}_{j} + \frac{5}{6} f^{-}_{j+1} - \frac{1}{6} f^{-}_{j+2}\right) \\ &+ \omega_0^{-}\left(\frac{11}{6} f^{-}_{j+1} - \frac{7}{6} f^{-}_{j+2} + \frac{2}{6} f^{-}_{j+3}\right)\end{aligned} \tag{24}$$

$$\phi_{conv^{n}_{i,j}} = -\frac{1}{\Delta x}\left[\left(\hat{f}^{+}_{j+\frac{1}{2}} - \hat{f}^{+}_{j-\frac{1}{2}}\right) + \left(\hat{f}^{-}_{j+\frac{1}{2}} - \hat{f}^{-}_{j-\frac{1}{2}}\right)\right] \tag{25}$$

- **Approximation of time**

For the time approximation of equation (13), we employed the third-order accurate TVD Runge-Kutta scheme to advance in time:

$$f^{(1)} = \gamma_1 f^n + \gamma_1' \Delta t^* L(f^n) \tag{26}$$

$$f^{(2)} = \gamma_2 f^n + \gamma_2' \left[f^{(1)} + \Delta t^* L(f^{(1)}) \right] \tag{27}$$

$$f^{n+1} = \gamma_3 f^n + \gamma_3' \left[f^{(2)} + \Delta t^* L(f^{(2)}) \right] \tag{28}$$

where: $\gamma_1 = 1$, $\gamma_2 = \frac{3}{4}$, $\gamma_3 = \frac{1}{3}$, $\gamma_1' = 1$, $\gamma_2' = \frac{1}{4}$, $\gamma_3' = \frac{2}{3}$ and Δt^* is the dimensionless time step. For further details see Gottlieb and Shu [66].

2.3. Numerical validation tests

To verify the accuracy and correctness of the in-house code used in this study, we have referenced the work carried out by Nishimura et al. [67], which corresponds to double-diffusive natural convection flow in a vertical rectangular enclosure. Their work is considered an excellent benchmark, extensively employed by many investigators (see, for instance, [68], [69], [70]) to check the validity and efficiency of computational codes.

The computational conditions in this study are as follows: the Prandtl number $\Pr = 1$, the Lewis number $Le = 2$, and the Rayleigh number $Ra = 10^5$. These values cover a range of buoyancy ratios ($R_\rho = 0.8$, 1 and 1.3) corresponding to various flow regimes. The same dimensions (aspect ratio $Ar = 0.5$) and grid resolution (31×41) as in the study by Nishimura et al. [67], were utilized for consistency and comparability.

Figure 2 provides a clear comparison between the numerical results of streamline, isotherm, and concentration plots obtained using the present code and those from Nishimura et al. [67]. The plots illustrate three distinct flow behaviors: compositionally dominated flow, thermally dominated flow, and oscillatory flow, corresponding to the buoyancy $R_\rho = 1.3$, $R_\rho = 0.8$ and $R_\rho = 1$, respectively. The comparison demonstrates good agreement with the results reported by Nishimura et al. [67], confirming the capacity and numerical accuracy of our computational code in simulating double-diffusive natural convection flow.

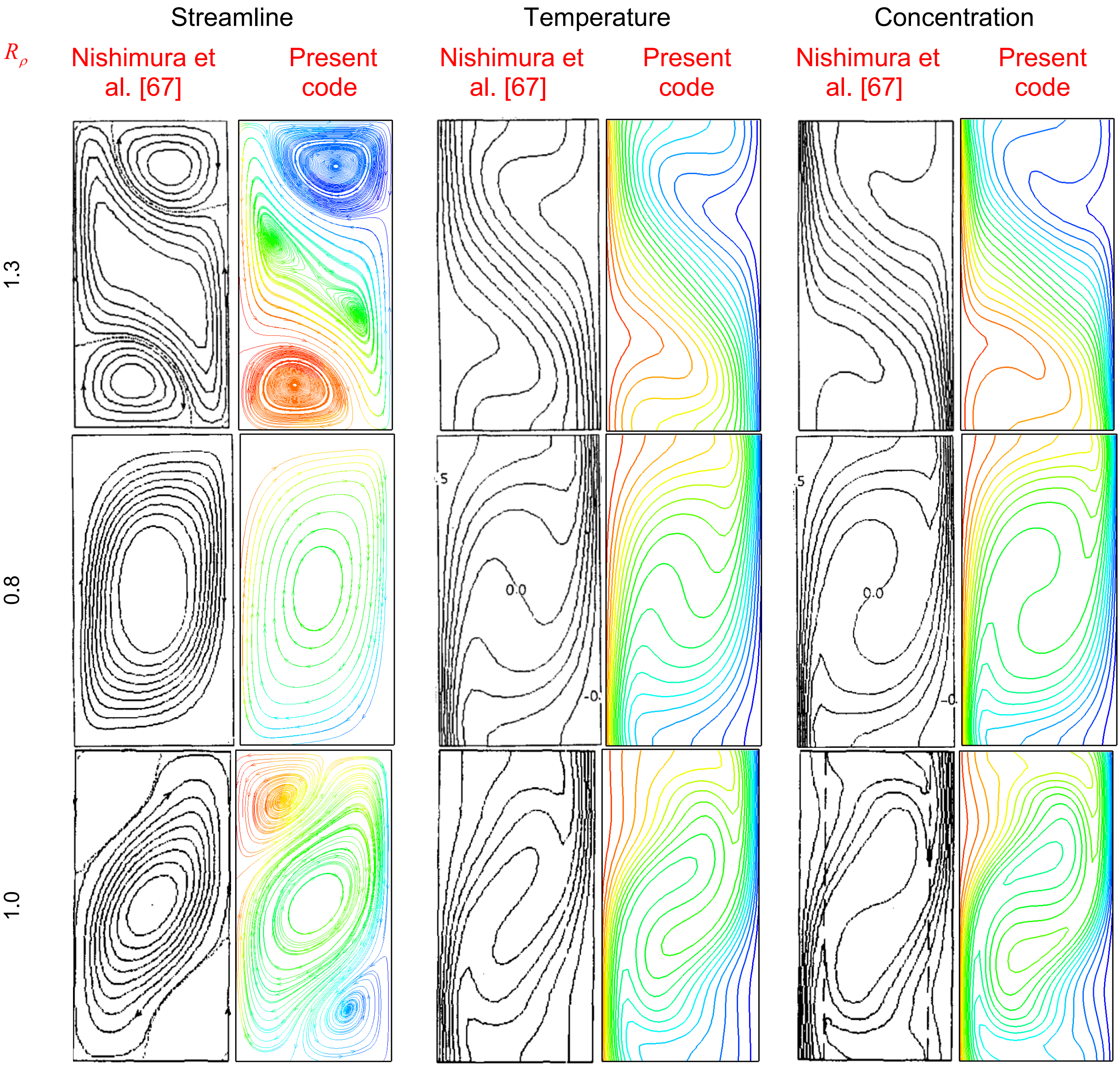

Figure 2. Comparisons between the results from the present code and the numerical results from Nishimura et al. [67].

Furthermore, our computational code is extensively used to solve double-diffusive salt fingers in our previous studies covering a wide range of buoyancy ratios $R_\rho = 1.5 - 20$. For each buoyancy ratio, the thermal Rayleigh number varies in the order of $Ra_T \sim 10^3 - 10^8$ [36], [54], [60]. The computational results have demonstrated excellent agreement with the previous laboratory experiments and numerical published works related to the oceanography field.

To assess the sensitivity of the results to the grid size changes, a grid independence study was conducted for computations involving the evolution of finger structures. The results of our numerical tests showed that the numbers of grids mesh 400×300 chosen as a typical resolution to solve the evolution pattern of finger convection in the enclosure. This grid size enables accurate capture of the finger structures.

3. Results and discussions

It is well known that the transport of salt is directly related to the dynamics of the fingers, which play a crucial role in the mixing process. Indeed, this section focuses on the evolution of the fingers to explain the mechanisms of mixing in detail. Specifically, we examine how the nonlinear equation of state affects the formation, dynamic, and interaction of the fingers, ultimately influencing the overall mixing behavior.

To assess the influence of the nonlinear equation of state, we consider three scenarios varying in the nonlinear parameter: a linear case ($\varepsilon = 0$), a weakly nonlinear case ($\varepsilon = 1$), and a highly nonlinear case ($\varepsilon = 3$).

3.1 Effect of nonlinear parameter on the flow structures and mixing properties

- **Reference case: Linear state equation ($\varepsilon = 0$)**

Let us firstly starts by examining the case corresponding to the linear state equation $\varepsilon = 0$which serves as a valuable reference, for understanding the effects induced by the nonlinear parameter on the salt transport process in fingering convection.

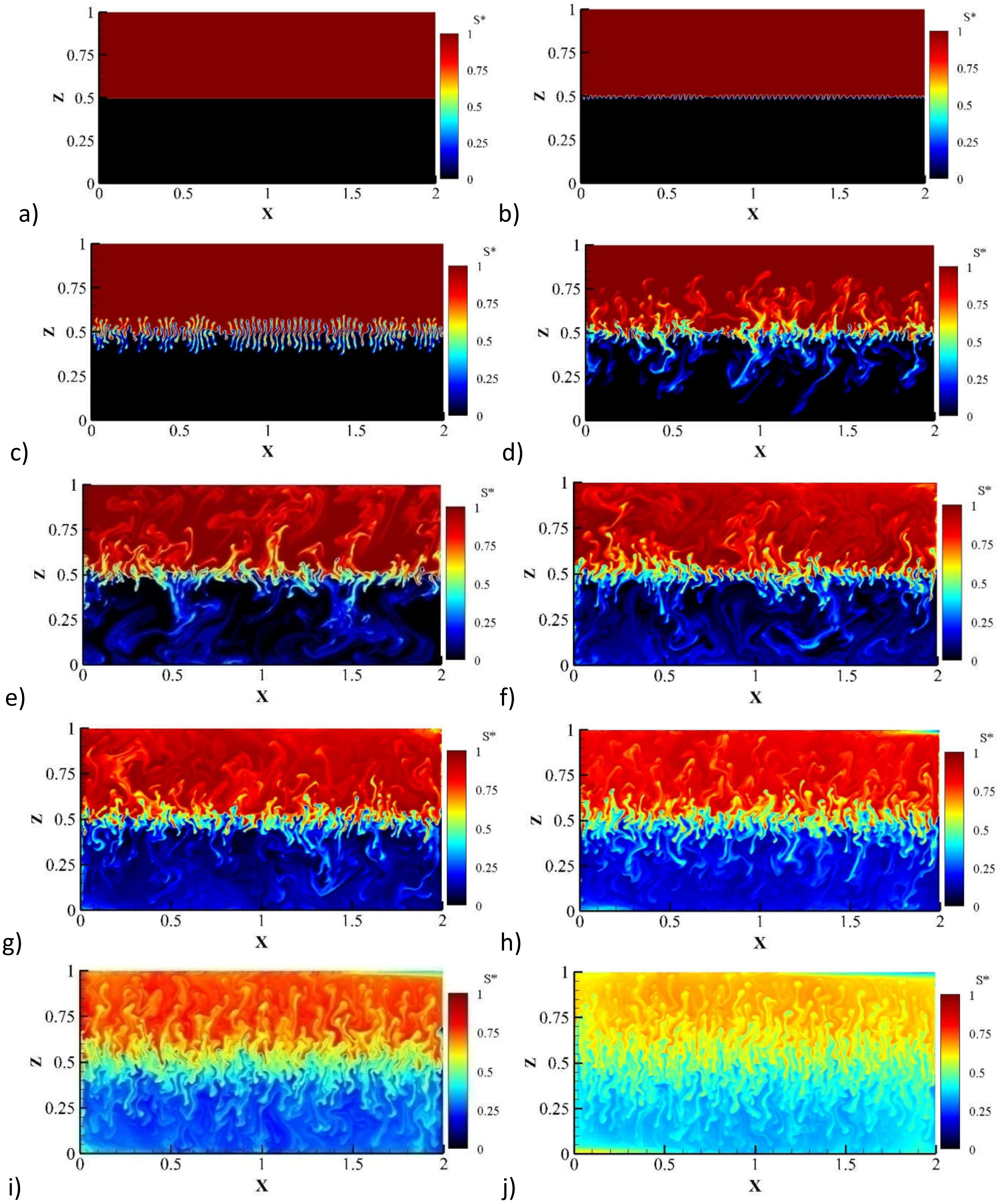

Figure 3. Evolution of salt-finger structures at high thermal Rayleigh numbers $Ra_T = 7 \times 10^8$ for the linear case $\varepsilon = 0$. Red regions represent regions with higher salinity and temperature, indicating hot and saline fluids, while blue regions represent regions with lower salinity and temperature, indicating cold and fresh fluids.

Figure 3 shows the instantaneous contours of the evolution of a salt fingers structure. A global overview of this figure indicates clearly that the dynamic and the evolution of salt fingers seem identical at the upper and lower layers; therefore, the system may be considered symmetric about the middle of the domain. Furthermore, the system dynamics exhibit several phenomena occurring during the evolution spatio-temporal of salt fingers which can be summarized in the following stages: (1) Stable, (2) Early, (3) Mature, and (4) Rundown.

Initially, figure 3 a depicts the stable stage, which is characterized by pure diffusion process through the separation interface also called "fingering interface," with no visible fingers in the system. Subsequently, small perturbations in the fluid induce undulations in the fingering interface. These undulations results in the formation of very thin finger-like structures, or filaments, with approximately 132 fingers. As we can see from the figure 3b, 66 are ascending, of which cold and fresh, while the other 66 are descending, of which hot and saline.

In the second or early-stage, salt finger begins to growth linearly as shown in figure 3c this stage is much faster as the density ratio is weaker. Hence, the fingers structures start to interact rapidly with one another and merged into finger conduits causing a new reorganization of fingers structures 'tree-like' see figure 3d.

The finger conduits mix well before reaching the horizontal boundaries and blooms, forming several branches. This branching allows for greater lateral spread of fluid than at earlier stages; hence, the system behavior becomes dynamically much more complicated.

As the fingers reach the horizontal boundaries, they accumulate along the top and bottom boundaries, leading to the formation of mixed layers. The fingers become hence sandwiched between these mixed layers, forming so-called the "finger zone," as shown in figures 3 e and f. The mixed layers, initially, are characterized by intense convective motion upon their formation, which prevents further growth of the fingers.

Figures 3 g and h reveal that the diffusion of salt intensifies in the finger zone with time between the saline ascending and fresh descending finger structures. The salt diffuses strongly laterally to adjacent fingers through the surfaces that form the fingers because the fingers are numerous and closely spaced.

As time progresses, the intensity of convection in the mixed layers decreases, allowing the fingers to extend once again, see figure 3 i.

During the rundown stage illustrated in figure 3 j, the mixing activity diminishes, and the system transitions into a state dominated by molecular diffusion. The diffusion mechanism plays a pivotal role in homogenizing the salt distribution and stabilizing the overall system. Ultimately, as diffusion dominates in the system, the salt finger structures begin to dissipate. The system hence becomes dynamically less active and the vertical salinity flux is negligible.

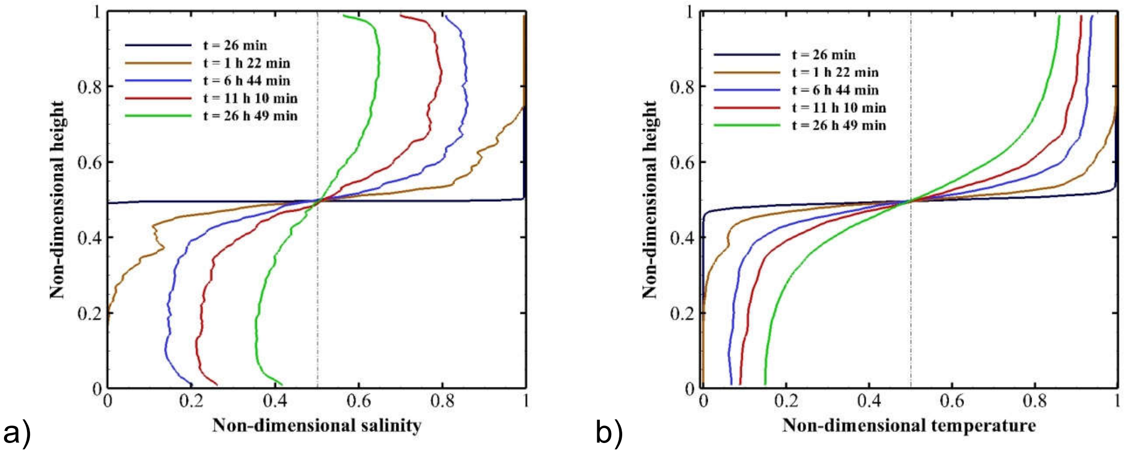

Figure 4. Horizontally averaged profiles of (a) salinity and (b) temperature at high thermal Rayleigh numbers $Ra_T = 7\times10^8$ for the linear case $\varepsilon=0$. Over time, the salinity profile becomes uniform within the layer, while the temperature profile retains a significant contrast between the layers.

Figure 4 displays the time evolution of horizontal averaged profiles of temperature and salinity for linear equation of state. The initial distributions of ($T*$, $S*$) components show stabilizing thermal gradients that counteract destabilizing salt gradients. These initial (T^*, S^*) distributions between the upper and lower layers lead to the triggering of convective motions in the fingering regime.

For ($\mathrm{t} \leq 26\,\mathrm{min}$), salt profiles are characterized by a very weak change in salt gradient near the mid-height of the computational domain. This means that the thickness of the fingering interface is small, and the exchange of salt between the upper and lower layers is mainly driven by diffusive processes.

It is noteworthy that all the profiles exhibit clear symmetry about the mid-height of the computational domain. Furthermore, the similarity in the distribution of salt profiles in the spread zone (the zone invaded by the fingers bounded between no-mixed layers $<S^*>=0$ and $<S^*>=1$) distribution implies that the velocities of rising and sinking fingers are equal.

As the mixed layers begin to thicken ($\mathrm{t} \geq 1\mathrm{h}\ 22\,\mathrm{min}$), the salt profile convects quickly towards an asymptotic value of salinity, approximately 0.5. This results in a uniform distribution of salinity in the system (i.e., salt gradient $\Delta S \sim 0$), ultimately forming stable layers.

The temperature profiles in figure 4 b also exhibit also symmetric about the center of the computational domain. By analyzing the temperature profiles, we can make the same observations as with the salinity profiles. However, the change in the slope of the spread zone indicates that the heat quantity being transported by fingers is less than that of the solute mass, implying that salt advecte more rapidly than heat.

Let us examine the mixing characteristics within the system, utilizing Probability Density Function PDF(S*) analysis to assess the quality of mixing outcomes arising from the development of salt fingers for linear equation state.

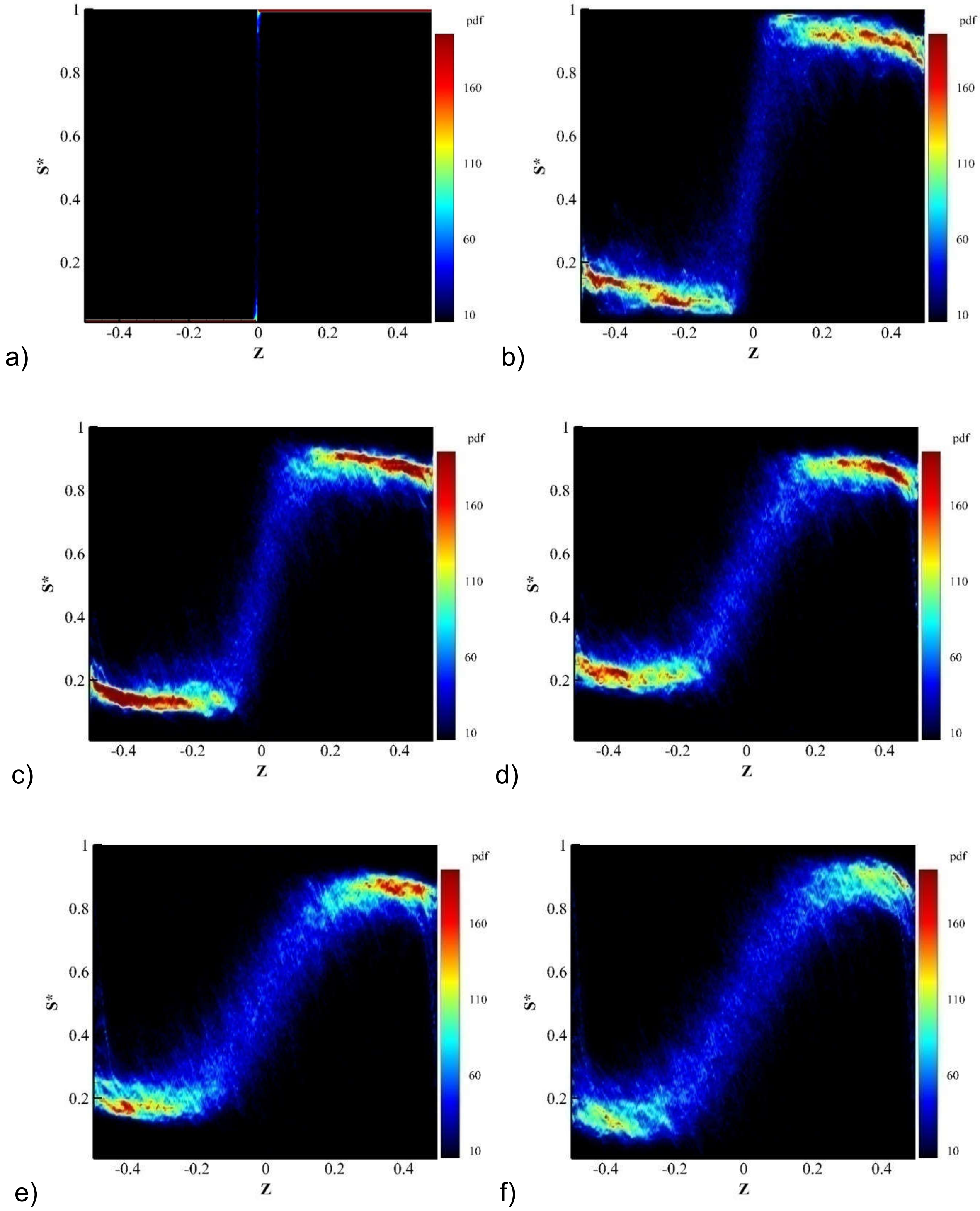

Figure 5. Evolution of the probability density function of salinity as a function of height at high thermal Rayleigh numbers $Ra_T = 7\times10^8$ and $R_\rho = 1.5$ for the linear case $\varepsilon = 0$, showing the phases of the mixing process. The figure illustrates the temporal changes in salinity distribution, highlighting the different stages of mixing and the development of distinct layers over time.

To facilitate the analysis as well as the interpretation of PDF(S*) plotting regarding the symmetry of the mixing evolution, we have shifted the origin position to the center of the computational domain.

Figure 5 illustrates the evolution of the PDF(S*) of the salt transported by the fingers. In figure 5 a, it is clear that there is a substantial probability of finding $S^*=1$ in the upper layer and $S^*=0$ in the lower layer. Conversely, a much weaker probability is observed in the middle of the computational domain for larger values of $0\leq S^*\leq 1$. This observation indicates that the mixing process within the system initiates through molecular diffusion through the fingering surface. With the development of finger structures, the enhancement of mixing quality becomes evident, attributed to the convective transport of salt between the upper and lower layers.

Three distinct mixing zones may be identified (figure 5 b and c): the upper zone, where a high probability of salt limitation occurs ($0.8\leq S^*\leq 0.9$); the lower zone characterized by a strong probability of salt ($0.1\leq S^*\leq 0.2$); and the middle zone, featuring significant salt diffusion across the fingering surface that forming the finger structures.

Within this middle zone, a wide range of weak PDF(S*) values ($0.2\leq S^*\leq 0.8$) is observed, defining the fingering zone that is sandwiched between the lower and upper zones. Additionally, it is noteworthy that the PDF(S*) values for $S^*=0$ and $S^*=1$ are both zero, indicating that fingers extended and reached the horizontal boundaries.

With the passage of time, salt accumulates near the boundaries, creating mixed layers that inhibit the further growth of finger structures and impede the transport of salt towards them. Moreover, the mixing process within the mixed layers ($-0.5 < Z <$ -

0.1 and $0.1 < Z < 0.5$) is notable, mainly due to the vigorous convection, as seen in figure 5 d.

The PDF(S*) in figure 5 e and f clearly illustrate a gradual decrease in mixing activity within the mixed layers, attributed to the diminishing convective intensity in these regions. Additionally, the thickness of the mixed layers decreases ($-0.5 < Z < -0.3$ and $0.3 < Z < 0.5$) due to the widening of the finger zone ($-0.2 < Z < 0.2$), which is characterized by a significant diffusion of the salt, representing the signature of finger regrowth.It is worth mentioning that there is a clear symmetry of mixing process within the system about the center of the computational domain.

- **High and weak nonlinear cases ($\varepsilon=1, \varepsilon=3$)**

A global view of the figure 6 reveals clearly that the nonlinear parameter causes a breakdown in the system's symmetry.

As in the linear case, for weak nonlinear case ($\varepsilon=1$) instability at the interface initiates undulation, leading hence to the formation of wavy finger structures. In the weakly nonlinear case, where the nonlinearity parameter $\varepsilon = 1$, the quadratic term ΔT^2 in the equation of state has a moderate effect on the density variation due to temperature changes. This condition allows us to analyze the behavior of both descending and ascending fingers. Descending fingers are typically colder and saltier than the surrounding fluid, leading to an increase in density. This increase is more pronounced for descending fingers due to the moderate enhancement in density caused by the quadratic term in the equation of state.

This moderate enhancement results in a stronger buoyancy force acting on the descending fingers, causing them to accelerate more rapidly.

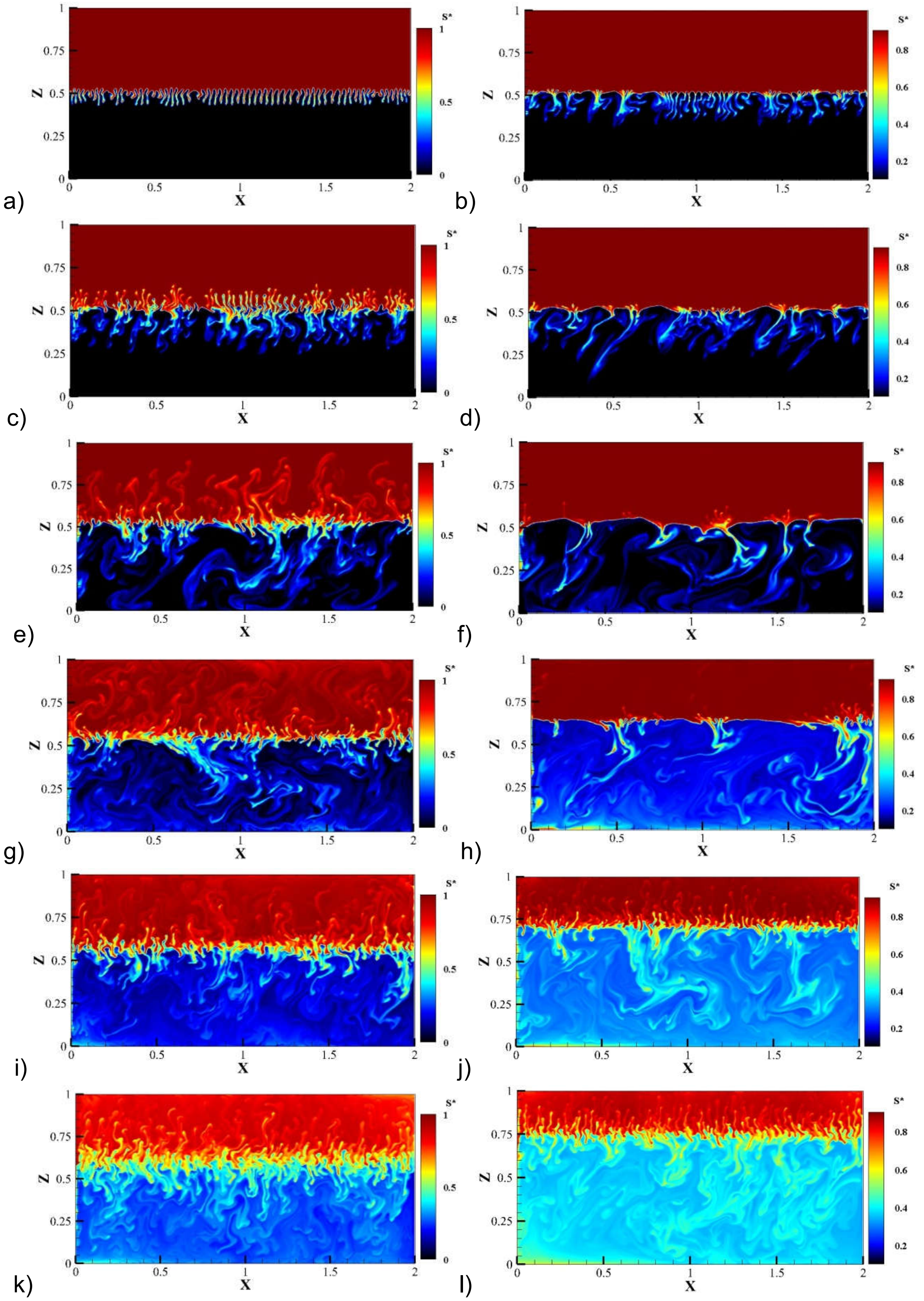

Figure 6. Evolution of salt-finger structures at high thermal Rayleigh numbers $Ra_T = 7\times10^8$ and $R_\rho = 1.5$ for the nonlinear cases. Red regions denote areas with higher salinity and temperature, representing hot and saline fluids, while blue regions indicate areas with lower salinity and temperature, representing cold and fresh fluids. The left panels correspond to the weakly nonlinear case ($\varepsilon = 1$), while the right panels correspond to the strongly nonlinear case ($\varepsilon = 3$).

The increased acceleration due to the stronger buoyancy force causes the descending fingers to become narrower. This narrowing effect is a common phenomenon in fluid dynamics, where stronger forces tend to create more focused, narrow structures. Consequently, the descending fingers grow faster under these conditions (see figure 6 a).

On the other hand, ascending fingers are typically warmer and less salty than the surrounding fluid, resulting in a decrease in density. The effect of the quadratic term ΔT^2 in the equation of state is also present for ascending fingers but is less pronounced due to the smaller temperature difference involved. As a result, the buoyancy force acting on ascending fingers is weaker, causing them to rise more slowly and develop less pronounced structures (see figure 6 a). This asymmetry in the behavior of descending and ascending fingers creates a convection pattern that exhibits some degree of asymmetry but is not extremely pronounced.

The descending fingers form tree-like structures early compared to the ascending ones, resulting in a significantly more dynamic behavior in the lower layer (see figure 6 c).

The figure 6 e shows that the descending fingers reach the bottom boundary early, leading to the premature formation of the lower mixed layer. Subsequently, the ascending fingers reach the upper boundary, interacting with it to merge and form the upper mixed layer.

In figure 7 a, the flow pattern reveals recirculation zones above and below the finger region, which is the result of convection occurring in both the upper and lower layers. These convection zones affect significantly transport and mixing of salt. Indeed, they pinch the finger zone and limit their growth. Thus, the finger zone remains suspended between these two convective layers and become more diffuse. In addition, it is apparent that convection is more intense in the lower layer than in the upper layer. This disparity in intensity leads in a slight displacement of the finger zone, initially located in the middle of the domain, towards $Z=0.55$ (figure 6 g and i).

Eventually, as the intensity of convection decreases, the fingers grow again, feeding the system and allowing for transport of salt between layers, as shown in figure 6 k. In this stage, the system becomes dominated by a diffusion process.

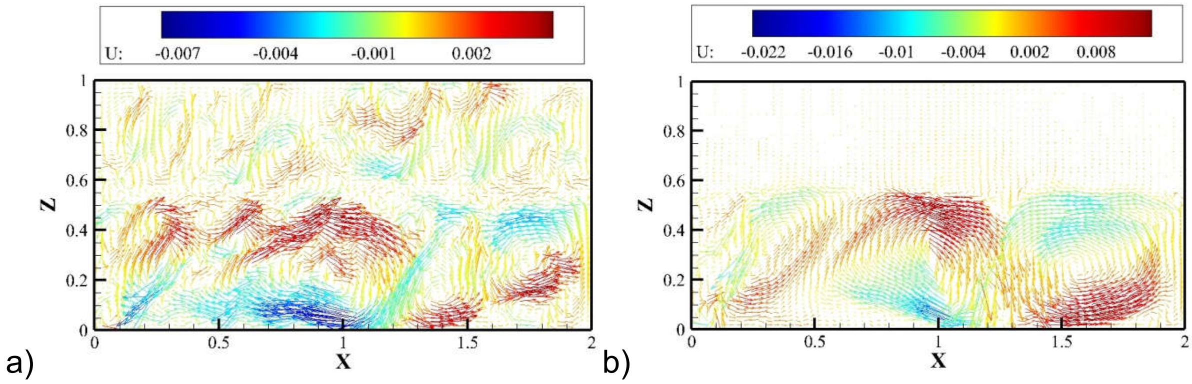

Figure 7. Contour of the velocity vector at high thermal Rayleigh number $Ra_T = 7\times10^8$ and $R_\rho=1.5$: The left panels correspond to the weakly nonlinear case ($\varepsilon=1$), while the right panels correspond to the strongly nonlinear case ($\varepsilon=3$).

In the highly nonlinear case ($\varepsilon=3$), the evolution pattern of the fingers differs significantly from that observed in the weakly nonlinear case. In this scenario, there is a clear asymmetry in the mechanism of salt transport, which occurs from the upper layer to the lower layer.

In the highly nonlinear case, where $\varepsilon=3$, the quadratic term ΔT^2 in the equation of state has a strong effect on the density variation due to temperature changes. This strong effect leads to a significant increase in density for descending fingers, which are colder and saltier than the surrounding fluid. The strong enhancement in density caused by the quadratic term results in a much stronger upward force on the descending fingers, causing them to accelerate rapidly. This rapid acceleration leads to even narrower descending fingers compared to the weakly nonlinear case.

Ascending fingers, being warmer and less salty, experience a decrease in density. The effect of the quadratic term is also present for ascending fingers but is less pronounced due to the smaller temperature difference. As a result, the upward force on ascending fingers remains relatively weak, causing them to rise slowly and develop even less pronounced structures. In the highly nonlinear case, the strong enhancement of buoyancy forces leads to much faster-growing and narrower descending fingers compared to ascending fingers (see figure 6 b). This results in a highly asymmetric convection pattern, with the system being dominated by the rapidly growing and narrow descending fingers, and the ascending fingers being strongly damped.

The descending fingers coalesce, merge, and reorganize into dense plumes (see figure 6 d and f) that exhibit high spatial and temporal variation, leading to the development of vigorous convection characterized by large convective cells that occupy the entire lower layer as shown in figure 7 b. Afterwards, any descending finger produced by the system is swept away and engulfed by these large convective cells. Moreover, we observe a reduction in the number of fingers, with the finger zone nearly vanishing along the interface separating the two layers (see figure 6 h). The fingering surface exhibits a partial return to its initial state. Additionally, there appears to be a deficit in the generation of new fingers.

In contrast, the upper layer devoid of fingers remains stagnant, acting as a reservoir that supplies the lower layer. As a result, the lower zone thickens as the upper layer is depleted, driven by strong convection. Indeed, we observe an unusual phenomenon: the finger zone, initially situated at the center of the domain, gradually moves upward and settles at $Z=0.70$ (see figure 6 j), resulting in a complete breakdown of the system's symmetry. It is noteworthy that the formation of the lower mixed layer is not prominent in this case due to the triggering of intense convection with larger-scale convective cells (see figure 7 b).This prevents salt from accumulating and settling at the bottom boundary during its formation, as shown in the figure 6 j. It is important to note that as the ascending fingers develop, salt begins to be transported from the lower layer to the upper layer, and hence, the finger zone stabilizes and ceases its upward displacement, settling at a height of $Z = 0.75$ (see figure 6 l). We also observe the delayed formation of the upper mixed layer, which decreases in thickness over time. These results can be observed more quantitatively by looking at the salt profiles in figure 8 b.

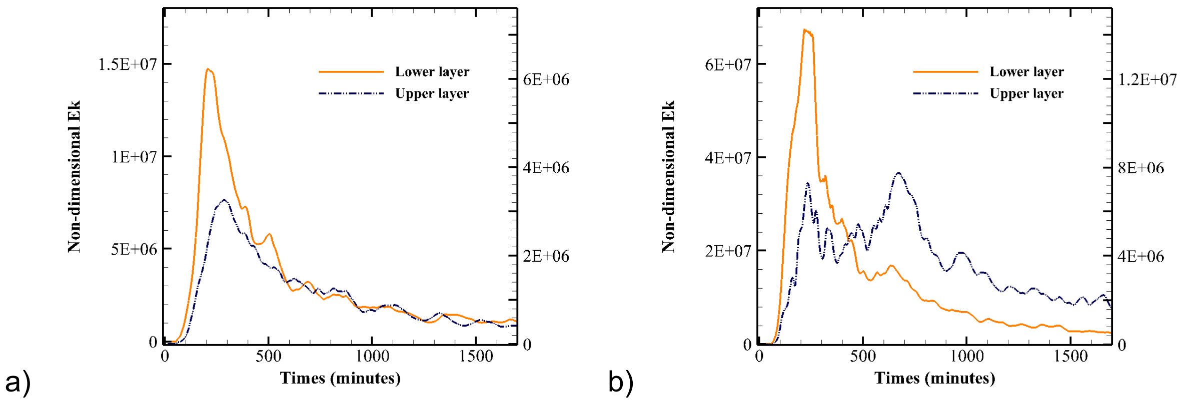

Figure 8. Plot of the kinetic energy E_k of the system as a function of time at high thermal Rayleigh number Ra$_T$ $Ra_T = 7\times10^8$ and $R_\rho = 1.5$: The left panels correspond to the weakly nonlinear case ($\varepsilon = 1$), while the right panels correspond to the strongly nonlinear case ($\varepsilon = 3$).The solid lines and the dashed lines represent the vertical kinetic energy averaged over all descending and ascending fingers, respectively.

To be more precise in analyzing the previous instantaneous results, we will examine the kinetic energy and horizontally average temperature and salinity profiles of the system. The non-dimensional kinetic energy denoted E_k is expressed as $E_k = \frac{1}{2} < U^2 + W^2 >$, where $< >$ indicate averaged domain, U and W are the horizontal and vertical velocity components.

The build-up of kinetic energy in the figure 8 indicates that the onset of finger instability is delayed in the upper layer compared to the lower layer. This delay is mainly due to the earlier development of descending fingers. Moreover, in the nonlinear cases, the large amount of potential energy available in the system is converts into kinetic energy by descending fingers. Hence, the potential energy converts quickly to kinetic energy, reaching its maximum magnitude in the lower layer compared to the upper layer for both cases ($\varepsilon=1, \varepsilon=3$). Additionally, the maximum magnitude of kinetic energy increases in both upper and lower layers as the nonlinear parameter increases. Interestingly, for the high linear case, in the upper layer, two obvious peaks are detected, see the figure 8 b. The first peak is obtained due to the release of the potential energy by the ascending fingers that boost the kinetic energy until it reaches its first maximum value. Subsequently, as the ascending fingers cease growing, there is a decrease in kinetic energy. Interestingly, there is a resurgence in the increase of kinetic energy in the upper layer, due principally to the increase in the level of the lower layer that invades approximately *20%* of the upper layer. This invasion reactivates and boosts the kinetic energy again until it attains its second peak, and finally, we notice a gradual decline the system’s in the kinetic energy across both upper and lower layers. This reduction is mainly due to the decreases in the finger zone motions and the mixed layers which means that the system tends towards equilibrium and become influenced by diffusive processes.

The salinity and temperature distributions are horizontally averaged to generate vertical profiles, as illustrated in figure 9. The initial distributions of the (T^*, S^*) components are symmetric about the mid-height of the computational domain, characterized by stabilizing thermal gradients counteracting destabilizing salt gradients. This distribution between the upper and lower layers leads to the generation of the fingers convection.

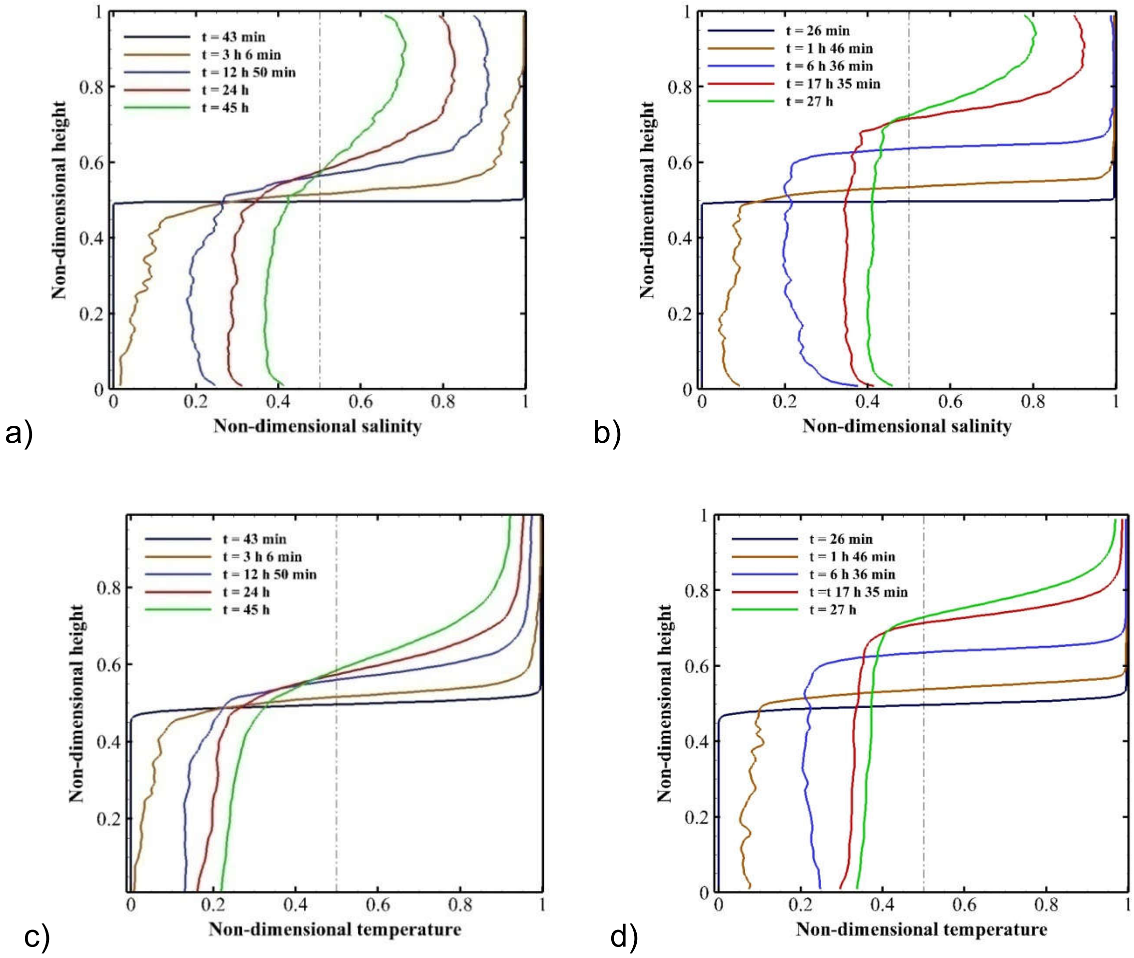

Figure 9. Horizontally averaged profiles of (a, b) salinity and (c, d) temperature at high thermal Rayleigh numbers $Ra_T = 7\times10^8$ and $R_\rho = 1.5$. The left panels show the profiles for the weakly nonlinear case ($\varepsilon = 1$), while the right panels depict the profiles for the strongly nonlinear case ($\varepsilon = 3$). These profiles illustrate the significant impact of the nonlinearity parameter ε on the distribution and dynamics of salinity and temperature in the fluid layers.

For the lowest nonlinear case $\varepsilon = 1$, for $t > 3\,\mathrm{h}$, the salinity values at the upper boundary remain close to $S^* = 1$, indicating that the fingers have not yet reached the top of the domain. In contrast, salinity starts to gradually increase from $S^* = 0$ which implies that the descending fingers reach the bottom of the domain earlier than the ascending ones.

Moreover, for $t > 12\,\mathrm{h}$, the averaged profiles clearly indicate that the upper zone consists of two regions: a fingering zone and a mixed layer whereas, in the lower layer, a single zone was identified, marked by the formation of a mixed layer, with the salt value remaining nearly constant, indicating a homogeneous distribution of salt. Indeed, the lower mixed layer zone thickens and encompassed the entire lower half of the domain while the thickness of the top mixed layer decreases with the growth of the finger zone that characterized by strong diffusion process. Consequently, finger zone takes place in the upper half of the domain and sandwiched between these mixed layers.

Over time, $t > 45\,\mathrm{h}$, the salt profile tends to convect vertically towards an asymptotic value of approximately $S^{*} = 0.5$, resulting in a uniform distribution of salinity in the system with contrast between the layers($\Delta S^{*} = 0$).

In the highest nonlinear case $\varepsilon = 3$, for $t > 1\,\mathrm{h}\,40\,\mathrm{min}$, the profiles indicate that in the lower half of the domain ($Z<0.5$) the salinity value changes rapidly, reaching values above zero. The averaged profiles distribution is nearly constant, indicating unevenly distributed of salt. This is mainly due to the convective cells generated by the earlier coalescence of the fingers in the lower layer, which mixed them thoroughly (figure 7 b). However, the profiles in the upper layer $0.5<Z<0.58$ (i.e. $\Delta Z = 0.8$) show a finger zone and for $Z>0.6$ the salinity value remains constant at its initial value of $S^{*}=1$, indicating that the ascending fingers in this zone is very slow and appears inhibited.

Intriguingly, for the highly nonlinear parameter $\varepsilon = 3$, the finger zone does not grow with time but instead moves upward, maintaining a consistently small thickness fixed at $\Delta Z = 0.8$. Therefore, the averaged profiles show clearly that the finger zone is confined between the pure upper unmixed salinity ($S^{*} = 1$) and lower mixed zones. Furthermore, for $t = 6\,\mathrm{h}\,36\,\mathrm{min}$, the lower homogeneous zone thickens as the upper layer is depleted, driven by strong convection. At $t = 17\,h\,35\,min$, the lower zone encompasses 70% of the domain, exhibiting a salinity value of $S^*=0.35$.We also clearly observe the formation of an upper mixed layer from $Z= 0.80$ to the end of the top boundary (i.e., $\Delta Z = 0.2$), which decreases in thickness to $\Delta Z = 0.1$ at $t = 27\,h$.

Upon examining the temperature profiles, it is observed that for the highly nonlinear case (figure 9 d), the heat transfer by descending fingers is almost the same to that of solute mass transport in the lower layer. However, for the upper layer, the quantity of heat transported by ascending fingers is less than that of the salinity.

For the weak nonlinear case (figure 9 c), the profiles clearly indicate that the heat quantity being advected vertically by ascending and descending fingers is less than that of the salinity.

We now turn to investigate how the nonlinearity parameter influences the quality and efficiency of mixing.

Figures 10 and 11 illustrate the evolution of the PDF(S*) of salinity for both weak and highly nonlinear cases. Regardless of the initial stage (not depicted), a global analysis reveals that mixing activity is more pronounced in the lower layer than in the upper layer, confirming the asymmetrical dynamics of finger evolution.

In figure 10 a, corresponding to the weak nonlinear case $\varepsilon=1$, three distinct mixing zones have been identified: zone 1 is bounded by $-0.5 < Z < 0$, zone 2 is bounded by $0 < Z < 0.15$, and zone 3 is bounded by $0.15 < Z < 0.5$.In the zone 1, mixing is driven by the formation of descending fingers that transport salt from the upper to lower layers. The early merging of descending fingers implies a faster mixing and enhances mixing activity in this zone. As the fingers reach the bottom of the domain, the probability of finding pure unmixed salinity ($S^* = 0$) remains zero. PDF(S*) also reveals that mixing activity is significantly close to the bottom due to the interaction of the lower mixed layer with the bottom boundary.

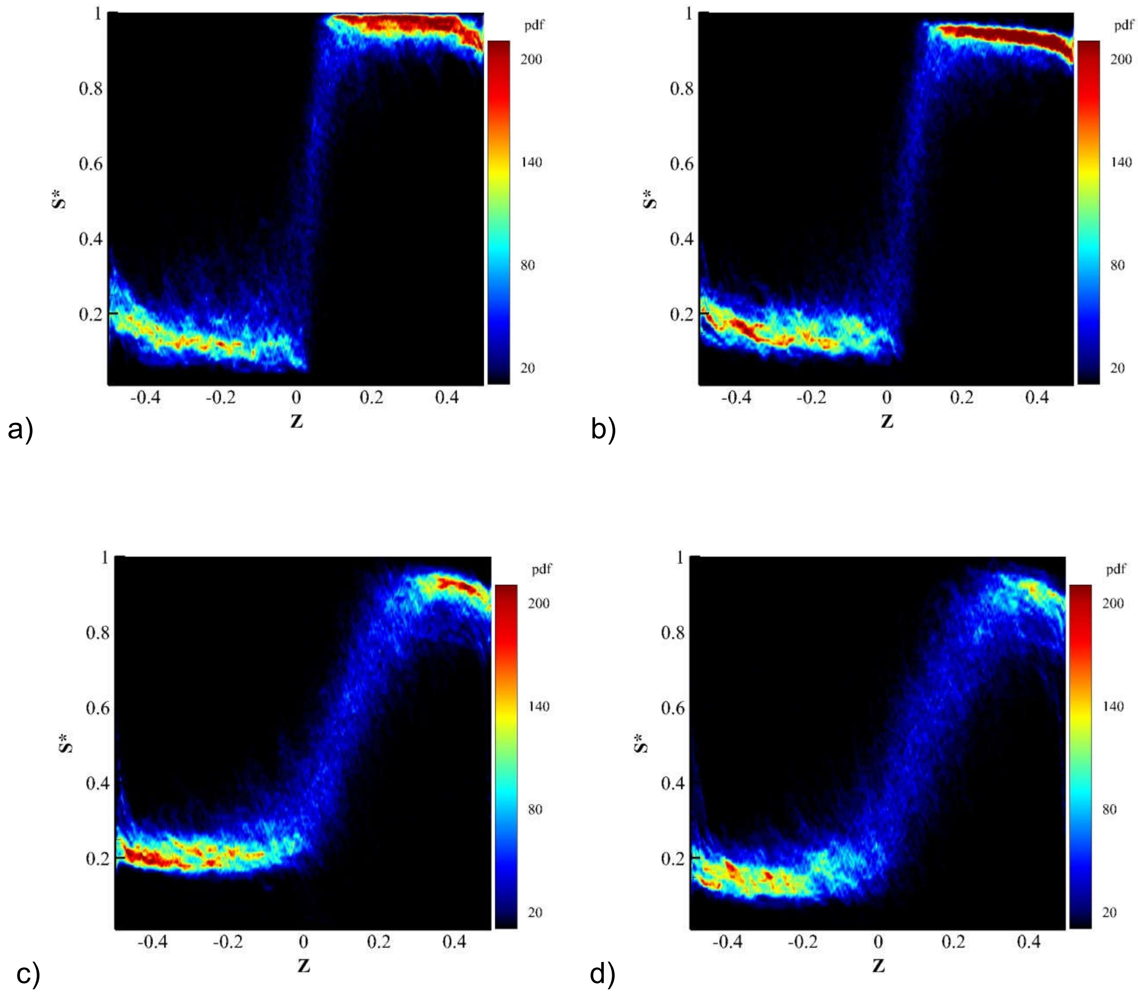

Figure 10. Evolution of the probability density function of salinity as a function of height at high thermal Rayleigh numbers $Ra_T = 7\times10^8$ and $R_\rho = 1.5$ for the nonlinear case ($\varepsilon = 1$). The figure highlights the effect of weak nonlinearity on the mixing process, illustrating how the distribution of salinity changes over time and showing the different stages of mixing and the development of distinct layers.

In the upper layer, figure 10 a shows that zone 2 is characterized by a wide band where salinity values are confined between 0.3 and 0.9, with a very low probability. Mixing in this zone is mainly driven by diffusive processes. In contrast, zone 3 exhibits a high probability of pure, unmixed salt ($S^* = 1$), indicating the absence of any mixing activity.

Over time, mixing activity intensifies, leading to thorough mixing of salt in the lower layer due to convection processes. This result in a better homogeneity of mixing in this zone, while the second zone extends and becomes much thinner and the mixture remains predominant by a diffusion process, see figure 10 b and c. However, we notice the increase in the mixing activity near the top of the domain due to the formation of upper mixed layer, indeed, the probability to find pure unmixed salinity ($S^* = 1$) become zero (figure 10 c). As time elapses, the intensity of convection in the mixed layer decreases in the upper layer, allowing the finger zone to begin transport again salute mass back towards the top of the domain. As a result, there is an increase in the thickness of the finger zone, accompanied by a decrease in mixing activity, with diffusion becoming the dominant process in the upper zone, as depicted in Figure 10 d.

In the highest nonlinear case $\varepsilon = 3$, the PDF(S*) also reveals three distinct mixing zones. Figure 11 a illustrates that the convective mixing dynamic predominantly occurs in the lower zone compared to the upper zone. The PDF(S*) distribution indicates that the probability to find pure unmixed salinity ($S^* = 0$) remains higher in the lower zone $-0.5 < Z < 0$, despite to the formation of the descending fingers. This means that the quantity of salt transported by the descending fingers from the upper layer ($S^* = 1$) to the lower layer ($S^* = 0$) is very weak. Additionally, we can also remark the existence of a band of salinity has values bounded between $0 \leq S^* \leq 0.1$ extended from the middle of the domain to the bottom boundary taking weak PDF(S*) values. This implies that the small amount of salt pumped from the upper zone is well mixed and becomes uniformly distributed throughout the lower half of the domain. In contrast, in the upper layer ($0 < Z < 0.5$), we observed that mixing in the second zone is predominantly diffusive and is confined to a thin layer of approximately $\Delta Z = 0.05$.

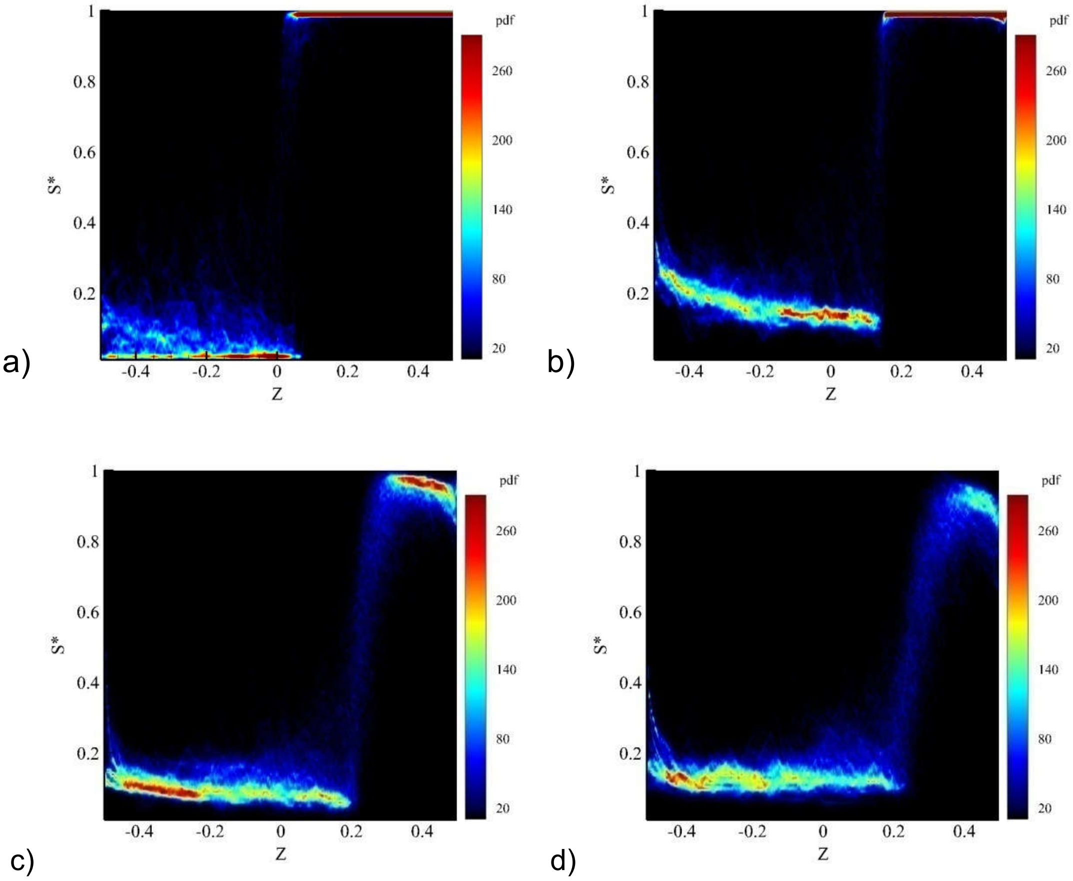

Figure 11. Evolution of the probability density function of the salinity at high thermal Rayleigh number $Ra_T = 7\times10^8$ and $R_\rho = 1.5$ for the nonlinear case ($\varepsilon = 3$). This figure emphasizes the impact of strong nonlinearity on the mixing process, illustrating how the distribution of salinity changes over time and showing the different stages of mixing and the development of distinct layers.

This zone is characterized by a broad range of salinity values with weak PDF(S*) values and it is followed by the third zone ($0.55<Z< 1$) where pure, unmixed salt ($S^* = 1$) is taking place because the ascending fingers are damped from growing under the effect of nonlinearity as shown in the figure 6 b and d, preventing the transport of salt to the upper zone.

It is interesting to note that the mixing process in the upper layer is inactive (i.e., unmixed salt $S^* = 1$) due to the lack of development of the ascending fingers (figure 11 b). Consequently, the upper layer serves as a nutrient reservoir for the lower layer via the descending fingers that transport salt from it towards the lower layer. Over time, the salt amount in the upper reservoir decreases, while the thickness of the lower mixing zone increases and extends up to $Z=0.2$ to cover 70% of the computational domain. Therefore, the second mixing zone moves from the center at $Z=0$ to $Z=0.2$, maintaining the same thickness of $\Delta Z \approx 0.1$. Consequently, the thickness of the third mixing zone decreases, occupying $\sim 25\%$ of the domain.

As time elapses, figure 11 c show, remarkably, a pronounced enhancement in mixing dynamics is observed near the horizontal boundaries, where salinity ranges from 0.2 to 0.3 in the bottom and from 0.8 to 0.9 in the top. This increased activity is mainly due to the significant interaction of the finger structures with horizontal boundaries. Furthermore, we observe that the probability of finding pure, unmixed salt $S^* = 0$, $S^* = 1$ in the lower and upper layers respectively is zero. This is corroborated by the instantaneous contours of the salinity in the figure 6 j.

Figure 11 d indicates that the mixing activity in the lower zone stays approximately constant, while the thickness of the second mixing zone increases with the formation of ascending fingers. The mixing activity in this zone is very weak and dominates by large diffusion of the salt. Additionally, the third mixing zone begins to decrease due to the increased growth of the fingers, and the intensity of mixing it decreases.

Indeed, for the highest nonlinear case ($\varepsilon=3$), the mixing efficiency appears to be qualitatively and quantitatively weak. This is due to a lack of a finger generation in the system, which plays a crucial role in transporting and exchanging salt between the lower and upper layers. On the other hand, the highly nonlinear parameter dampens and delays the formation of ascending fingers. In addition, any descending fingers that do form are quickly disrupted by strong convection cells in the lower zone.

4. Conclusion

In this study, we investigated the impact of the equation of state's nonlinearity on the evolution of double-diffusive finger convection and the mixing process through numerical simulations. We employed the finite volume method with high-accuracy schemes to solve the governing equations at low buoyancy ratios and high thermal Rayleigh numbers. The results obtained from the simulations indicate that the nonlinearity parameter (ε) plays a significant role in the formation structure of fingers, dynamics, and the transport processes of salt and heat in double-diffusive finger convection. Our findings can be summarized as follows:

1. **Impact on fingers dynamic:** Increasing the nonlinear parameter significantly enhances the buoyancy force acting on descending fingers compared to ascending fingers. This result in narrower and faster-growing descending fingers, while ascending fingers is appreciably damped, growing more slowly but with greater width. This pronounced asymmetry in finger development leads to distinct convective patterns between the upper and lower layers. Additionally, we observed a clear displacement of the fingering interface, a phenomenon that becomes more pronounced with increasing nonlinearity. The displacement of the fingering interface halts and stabilizes once the growth of ascending fingers commences.
2. **Impact on mixed layers:** In contrast to the linear case, where the upper and lower mixed layers have the same thickness, the differences in finger development in the nonlinear cases significantly affect the formation of mixed layers. Indeed, in the nonlinear cases, the thickness of the upper mixed layer decreases as the nonlinear parameter increases.

3. **Impact on mixing efficiency:** Analysis of the probability density function of salinity PDF(S*) reveals that the amount of salt transported by descending fingers from the upper to the lower layer decreases as the nonlinear parameter increases. This indicates a reduction in mixing efficiency with higher nonlinear parameter values, implying that increased nonlinearity hinders effective salt transport and mixing

Overall, our findings contribute to a deeper understanding of the complex dynamics of double-diffusive finger convection and highlight the importance of considering the nonlinearity of the equation of state in predicting transport processes and mixing proprieties in natural and engineered systems.

Nomenclature

Ar	enclosure aspect ratio $=B/H$
H	height of enclosure
B	width of enclosure
g	gravitational acceleration
p,P	dimensional and dimensionless pressures
T,T^*	dimensional and dimensionless temperatures
T_T,T_B	temperature of top and bottom layers
S,S^*	dimensional and dimensionless salinities
S_T,S_B	salinity of top and bottom layers
t,t^*	dimensional and dimensionless times
$\Pr, Sc$	Prandtl and Schmidt numbers
k_T,k_S	coefficient of thermal and salt diffusivities
R_ρ	density stability ratio
R_f	buoyancy flux ratio
T_0,S_0	reference temperature and salinity
Ra_T,Ra_S	thermal and salinity Rayleigh numbers
U,W	dimensionless horizontal and vertical velocity components
u,w	dimensional horizontal and vertical velocity components
X,Z	dimensionless Cartesian coordinates
x,z	Cartesian coordinates
d_i	linear weight for stencil i
IS_i	smoothness indicator for stencil i
$\hat{f}$	flux function
$\hat{f}_{j+\frac{1}{2}}$	reconstruct fluxes
$L(f)$	spatial discretization operator

Greek symbols

β_{T_1},β_{T_2}	linear and nonlinear thermal expansion coefficients
$\Delta\rho$	initial density difference between the two layers
ΔS	initial salinity difference between the two layers
ΔT	initial temperature difference between the two layers
$\Delta t,\Delta t^*$	dimensional and dimensionless time steps
ρ,ρ_0	dimensional and reference densities
ε	nonlinearity parameter
ν	kinematic viscosity
ϕ_{diff}	diffusive terms
ϕ_{conv}	nonlinear convective terms
α_i	Unnormalized weight for stencil i
σ	Small parameter to avoid division by zero
ω_i	Normalized weight for stencil i
γ_1	Weight for f^n in the first stage
γ_1'	Weight for the intermediate solution in the first stage
γ_2	Weight for f^n in the second stage
γ_2'	Weight for the intermediate solution in the second stage
γ_3	Weight for f^n in the third stage
γ_3'	Weight for the intermediate solution in the third stage

Subscripts and superscripts

$*$	dimensionless quantity
0	initial value
j	node indices
i	stencil index (0, 1, or 2)
$\pm$	approximation from the right and left, respectively
n	time level
$n+1$	next time level
(1)	Intermediate solution after the first stage
(2)	Intermediate solution after the second stage

5. References

[1] R.W. Schmitt, The characteristics of salt fingers in variety of fluid systems, including stellar interiors, liquid metals, oceans, and magmas, Phys. Fluids,26(9), 2373-2377 (1983).

[2] J. Olsthoorn, E.W. Tedford, G.A. Lawrence, Salt-fngering in seasonally ice-covered lakes, Geophys. Res. Lett. (2022).

[3] A. Oschlies, H. Dietze, and P. Kahler, Salt-finger driven enhancement of upper ocean nutrient supply, Geophys. Res. Lett., 30, 2204, (2003).

[4] F. Suárez, S.W. Tyler, A.E. Childress, A fully coupled, transient double-diffusive convective model for salt-gradient solar ponds, Int. J. Heat Mass Transfer., 53, 1718-1730, (2010).

[5] H. Emami-Meybodi, H. Hassanzadeh, C.P. Green,J. Ennis-King, Convective dissolution of CO_2 in saline aquifers: Progress in modelingand experiment, Int. J. Greenhouse Gas Control, 40, 238-266, (2015)

[6] J.S. Turner, I.H. Campbell, Convection and mixing in magma chambers , Earth-Sci Rev. 23, 255-352, (1986).

[7] P. Garaud, A. Kumar, and J. Sridhar, The Interaction between Shear and Fingering (Thermohaline) Convection, The Astrophysical Journal, 879, Number 1 (2019).

[8] M.E. Stern, The ‘salt fountain’ and thermohaline convection. Tellus, 12, 172-175, (1960).

[9] J.T.H. Andres and S.S.S. Cardoso, Onset of convection in a porous medium in the presence of chemical reaction,Phys. Rev. E 83, 046312 (2011).

[10] H. Yasmin, S. Akram, M. Athar, K. Saeed, A. Razia, J.G. Al-Juaid, Impact of multiple slips on thermally radiative peristaltic transport of Sisko nanofluid with double diffusion convection, viscous dissipation, and induced magnetic field, Nanotechnology Reviews 13 (1), 20240004, (2024).

[11] S. Bilal, S. Akram, K. Saeed, M. Athar, A. Riaz, A. Razia, A computational simulation for peristaltic flow of thermally radiative sisko nanofluid with viscous dissipation, double diffusion convection and induced magnetic field, Numerical Heat Transfer, Part A: Applications, 1-22, (2024).

[12] S. Akram, M. Athar, K. Saeed, M.Y. Umair, T. Muhammad, Mechanism of double diffusive convection due to magnetized Williamson nanofluid flow in tapered asymmetric channel under the influence of peristaltic propulsion and radiative heat transfer, International Journal of Numerical Methods for Heat & Fluid Flow 34 (2), 451-472, (2024).

[13] Y. Khan, S. Akram, M. Athar, K. Saeed, A. Razia, A. Alameer, Mechanism of Thermally Radiative Prandtl Nanofluids and Double-Diffusive Convection in Tapered Channel on Peristaltic Flow with Viscous Dissipation and Induced Magnetic Field. CMES-Computer Modeling in Engineering & Sciences 138 (2), (2024).

[14] S. Akram, M. Athar, K. Saeed, A. Razia, T. Muhammad, Role of thermal radiation and double-diffusivity convection on peristaltic flow of induced magneto-Prandtl nanofluid with viscous dissipation and slip boundaries, Journal of Thermal Analysis and Calorimetry 149 (2), 761-776, (2024).

[15] K. Saeed, S. Akram, A. Ahmad, Outcomes of partial slip on double-diffusive convection on peristaltic waves of Johnson–Segalman nanofluids under the impact of inclined magnetic field, Arabian Journal for Science and Engineering 48 (12), 15865-15881, (2023).

[16] S. Akram, M. Athar, K. Saeed, A. Razia, Influence of an induced magnetic field on double diffusion convection for peristaltic flow of thermally radiative Prandtl nanofluid in non-uniform channel, Tribology International 187, 108719, (2023).

[17] S. Akram, A. Razia, MY Umair, T Abdulrazzaq, RZ Homod, Double‐diffusive convection on peristaltic flow of hyperbolic tangent nanofluid in non‐uniform channel with induced magnetic field, Mathematical Methods in the Applied Sciences 46 (10), 11550-11567, (2023).

[18] S. Akram, M. Athar, K. Saeed, A. Razia, T. Muhammad, Hybridized consequence of thermal and concentration convection on peristaltic transport of magneto Powell–Eyring nanofluids in inclined asymmetric channel, Mathematical Methods in the Applied Sciences 46 (10), 11462-11478, (2023).

[19] S. Akram, K. Saeed, M. Athar, A. Razia, A. Hussain, I Naz, Convection theory on thermally radiative peristaltic flow of Prandtl tilted magneto nanofluid in an asymmetric channel with effects of partial slip and viscous dissipation, Materials Today Communications 35, 106171, (2023).

[20] S. Akram, M. Athar, K Saeed, A Razia, T Muhammad, HA Alghamdi, Mechanism of Double-Diffusive Convection on Peristaltic Transport of Thermally Radiative Williamson Nanomaterials with Slip Boundaries and Induced Magnetic Field, Nanomaterials 13 (5), 941, (2023).

[21] S. Akram, M. Athar, K. Saeed, A Razia, Theoretical analysis of partial slip on double-diffusion convection of Eyring-Powell nanofluids under the effects of peristaltic propulsion and inclined magnetic field, Journal of Magnetism and Magnetic Materials 569, 170445, (2023).

[22] S. Akram, M. Athar, K. Saeed, A. Razia, T. Muhammad, HA Alghamdi, Mathematical simulation of double diffusion convection on peristaltic pumping of Ellis nanofluid due to induced magnetic field in a non-uniform channel, Journal of Magnetism and Magnetic Materials 569, 170408, (2023).

[23] S. Akram, M. Athar, K. Saeed, A. Razia, T. Muhammad, A. Hussain, Hybrid double-diffusivity convection and induced magnetic field effects on peristaltic waves of Oldroyd 4-constant nanofluids in non-uniform channel, Alexandria Engineering Journal 65, 785-796, (2023).

[24] K. Saeed, S. Akram, A. Ahmad, M. Athar, A. Razia, T. Muhammad, Impact of slip boundaries on double diffusivity convection in an asymmetric channel with magneto tangent hyperbolic nanofluid with peristaltic flow, ZAMM Journal of Applied Mathematics and Mechanics,103(231), (2023).

[25] M. Gnanasekaran, A. Satheesh, Double-diffusive mixed convection with four heated square blocks for different working fluids in a square cavity. Numerical Heat Transfer, Part B: Fundamentals, 1–25 (2023). https://doi.org/10.1080/10407790.2023.2265550

[26] G. Manogaran, S. Anbalagan, Effect of magnetohydrodynamics and buoyancy ratio on thermosolutal double diffusion mixed convection in a cavity filled with liquid potassium alloy and Taguchi optimization with a linear regression model. Numerical Heat Transfer, Part A: Applications, 1–25. (2023). https://doi.org/10.1080/10407782.2023.2278707

[27] M. Gnanasekaran, A. Satheesh,Numerical simulation of MHD double-diffusive mixed convection in a closed cavity filled with liquid potassium alloy: Incorporating thermosolutal source,Case Studies in Thermal Engineering,Volume 52,2023,103772,ISSN 2214-157X,https://doi.org/10.1016/j.csite.2023.103772.

[28] M. Gnanasekaran, A. Satheesh, Influence of Joule heating and magneto-hydrodynamic on double diffusion mixed convection in a cavity with liquid sodium-potassium alloy and discrete thermosolutal source. Numerical Heat Transfer, Part A: Applications, 1–24 (2024). https://doi.org/10.1080/10407782.2024.2304043

[29] N.R. Devi, M. Gnanasekaran, A. Satheesh, P.R. Kanna, J. Taler, D.S. Kumar, D. Taler, T. Sobota,Double-diffusive mixed convection in an inclined square cavity filled with nanofluid: A numerical study with external magnetic field and heated square blockage effects,Case Studies in Thermal Engineering,Volume 56,2024,104210,ISSN 2214-157X,https://doi.org/10.1016/j.csite.2024.104210.

[30] R.W. Schmitt, Observational and laboratory insights into salt-finger convection, Prog. Oceanogr., 56, 419-433, (2003).

[31] A. Traxler, S. Stellmach, P. Garaud, T. Radko, and N. Brummell, Dynamics of fingering convection. Part 1 Small-scalefluxes and large-scale instabilities,J. Fluid Mech. 677, 530-553 (2011).

[32] E. Kunze, Limits on growing, finite-length salt fingers: A Richardson number constraint,J. Mar. Res. 45, 533-556, (1987).

[33] R.W. Schmitt, Triangular and asymmetric salt fingers. Journal of Physical Oceanography, 24, 855-860 (1994).

[34] E. Kunze, A review of salt-fingering theory, Prog. Oceanogr. 56, 399-417, (2003).

[35] M. E. Stern, and T. Radko, The salt finger amplitude in unbounded T–S gradient layers. J. Mar. Res., 56,157-196, (1998).

[36] R. Ouzani, Z. Alloui,Numerical study of two-dimensional salt-finger convection,Materials Today: Proceedings, 30, 833-837, (2020).

[37] J. Yoshida, and H. Nagashima,Numerical experiments on salt-finger convection, Progress in Oceanography, 56 ,435-459, (2003).

[38] R. Krishnamurti, Double-diffusive transport in laboratory thermohaline staircases. J. Fluid Mech. 483, 287–314, (2003).

[39] J.Taylor, and G. Veronis, Experiments on double-diffusive sugar-salt fingers at high stability ratio, J. Fluid Mech.,321, 315-333, (1996).

[40] M. Kellner, and A. Tilgner, Transition to finger convection in double-diffusive convection. Phys. Fluids, 26, 094103 (2014).

[41] C.Y. Shen, and G. Veronis, Numerical simulation of two-dimensional salt fingers, J.Geophys. Res., 102, 23131-23143 (1997).

[42] K.R. Sreenivas, O.P. Singh and J. Srinivasan, On the relationship between finger width, velocity, and fluxes in thermohaline convection. Phys. Fluids, 21, 26601-26615, (2009).

[43] J.S. Turner, Salt fingers across a density interface, Deep-Sea Res., 14, 599,(1967).

[44] T.M. Özgökmen, O.E. Esenkov and D.B. Olson, A numerical study of layer formation due to fingers in double-diffusive convection in a vertically-bounded domain.J. Mar. Res., 56, 463-487, (1998).

[45] R.W. Schmitt, The growth rate of supercritical salt fingers, Deep-Sea Res., Part A, 26, 23,(1979).

[46] T.J. McDougall and J.R. Taylor, Flux measurements across a finger interface at low values of the stability ratio, J. Mar. Res., 2, 1 (1984).

[47] D. Kelly, Oceanic thermohaline staircase," Ph.D. thesis, Dalhousie University, 1986.

[48] E. Kunze, Limits on growing, finite-length salt fingers: A Richardson number constraint. Mar. Res. 45, 533-556, (1987).

[49] J. D. Boyd and H. Perkins, Characteristics of the thermohaline steps off the northeast coast of South America,Deep-Sea Res., Part A **34**, 337, (1987).

[50] J. R. Taylor and P. Bucens, Laboratory experiments on the structure of salt fingers,Deep-Sea Res., Part A **36**, 1675 1989.

[51] C.Y. Shen, Heat-salt finger fluxes across a density interface, Phys. Fluids, 5, 2633-2643, (1993).

[52] C.Y. Shen, Equilibrium salt-fingering convection, Phys. Fluids, 7, 706, (1995).

[53] O.P. Singh and J. Srinivasan, Effect of Rayleigh numbers on the evolution of double-diffusive salt fingers. Phys. Fluids, 26, 062104-062118 (2014).

[54] R. Ouzani, Z. Alloui,S. Khelladi , and M. SpecklinDynamics of fingering convection: a numerical study,Environmental Fluid Mechanics, (2022).

[55] J. Olsthoorn, E. W. Tedford and G. A. Lawrence, The cooling box problem: convection with aquadratic equation of state, J. Fluid Mech.918(2021).

[56] J. Olsthoorn, E. W. Tedford, G. A. Lawrence, Salt-fingering in seasonally ice-covered lakes. Geophysical Research Letters, 49(2022).

[57] T.J. McDougall, Double-diffusive convection with a non-linear equation of state. Part II. Laboratory experiments and their interpretation, Prog. Oceanogr. 10, 91, (1981).

[58] R. W. Schmitt, Flux measurements at an interface, J. Mar. Res. 37, 419, (1979).

[59] T. M. Özgökmen, and O. E. Esenkov, Asymmetric salt fingers induced by a nonlinear equation of state, Physics of Fluids, 10, 1882, (1998).

[60] R. Ouzani, S. Khelladi, Numerical study of salt fingers dynamics: Effects of the density inversion, Therm. Sci. Eng. Prog.40, 101770, 2023.

[61] F. Oueslati, B. Ben-Beya, T. Lili, Double-diffusive natural convection and entropy generation in an enclosure of aspect ratio 4 with partial vertical heating and salting sources, Alex. Eng. J. 52, 605-625, (2013)

[62] Y. Yang, E. P. van der Poel, R. Ostilla-Mónico, C. Sun, R. Verzicco, S. Grossmann and D. Lohse, Salinity transfer in bounded double diffusive convection, J. Fluid Mech., 768 , 476-491, (2015).

[63] Y. Yang, R. Verzicco, and D. Lohse, Scaling laws and flow structures of double diffusive convection in the finger regime. J. Fluid Mech. 802, 667-689, (2016).

[64] C.W. Shu, Highorder ENO and WENO schemes for computational fluid dynamics, in High-Order Methods for Computational Physics, T.J. Barth and H. Deconinck, editors, Lecture Notes in Computational Science and Engineering, Springer, 9, 439-582, (1999).

[65] C.W. Shu, Essentially non-oscillatory and weighted essentially non-oscillatory schemes for hyperbolic conservation laws, in Advanced Numerical Approximation of Nonlinear Hyperbolic Equations, Lecture Notes in Math. 1697, Springer-Verlag, Berlin, 325-432, (1998).

[66] S. Gottlieb, C.W. Shu, Total variation diminishing Runge–Kutta schemes, Math.Comput., 67,73-85, (1998).

[67] T. Nishimura, M. Wakamatsu, A.M. Morega, Oscillatory double diffusive convection in a rectangular enclosure with combined horizontal temperature and concentration gradients, Int J Heat Mass Transfer, 41(11), 1601-1611, (1998).

[68] Q. Qin, Z.A. Xia, Zhen F. Tian. High accuracy numerical investigation of double-diffusive convection in a rectangular enclosure with horizontal temperature and concentration gradients, Int. J. Heat Mass Transfer, **71**, 405–423, (2014).

[69] A. J. Chamkh, H. Al-Naser Hydromagnetic double-diffusive convection in a rectangular enclosure with opposing temperature and concentration gradients, Int. J. Heat Mass Transfer, **45,** 2465-2483, (2002).

[70] A.A.A.A. Al-Rashed, H.F. Oztop, L. Kolsi, A. Boudjemline, M. A. Almeshaal, M. E. Ali, Ali Chamkha. CFD study of heat and mass transfer and entropy generation in a 3D solar distiller heated by an internal column. Int. J. Mech. Sci. **152**, 280-288 (2019).